Development of a stoichiometric magnesium potassium phosphate cement (MKPC) for the immobilization of powdered minerals

M. de Campos, Catherine Davy, Nora Djelal, Murielle Rivenet, J. Garcia

▶ **To cite this version:**

M. de Campos, Catherine Davy, Nora Djelal, Murielle Rivenet, J. Garcia. Development of a stoichiometric magnesium potassium phosphate cement (MKPC) for the immobilization of powdered minerals. Cement and Concrete Research, 2021, Cement and Concrete Research, 142, pp.106346. 10.1016/j.cemconres.2020.106346 . hal-04442677

HAL Id: hal-04442677
https://hal.univ-lille.fr/hal-04442677

Submitted on 22 Jul 2024

HAL is a multi-disciplinary open access archive for the deposit and dissemination of scientific research documents, whether they are published or not. The documents may come from teaching and research institutions in France or abroad, or from public or private research centers.

L'archive ouverte pluridisciplinaire **HAL**, est destinée au dépôt et à la diffusion de documents scientifiques de niveau recherche, publiés ou non, émanant des établissements d'enseignement et de recherche français ou étrangers, des laboratoires publics ou privés.

Distributed under a Creative Commons Attribution - NonCommercial 4.0 International License

Version of Record: https://www.sciencedirect.com/science/article/pii/S0008884620316264
Manuscript_cd1e5f8aa2c3e90096ae1dc8b6ca73bd

Submitted to Cement and Concrete Research November 20th, 2020

Development of a stoichiometric magnesium potassium phosphate cement (MKPC) for the immobilization of powdered minerals

M. De Campos[a*], C. A. Davy[a], N. Djelal[a], M. Rivenet[a], J. Garcia[b]

[a] Univ. Lille, CNRS, Centrale Lille, Univ. Artois, UMR 8181 - UCCS - Unité de Catalyse et Chimie du Solide, F-59000 Lille, France
[b] Orano, 125, Avenue de Paris, 92320, Châtillon, France

[*]corresponding author: matthieudcampos@gmail.com

Abstract: Ordinary Portland Cement (OPC)-based materials are not systematically adapted for immobilizing industrial hazardous waste, e.g. for aluminium powder or plutonium waste sludge. In such case, Magnesium potassium Phosphate Cements (MKPC) represent an interesting alternative.

The originality of this research is to develop a formulation of a MKPC paste for hazardous waste immobilization, which incorporates a maximum amount of such waste, preferably in powdered form. To this purpose, a stoichiometric MKPC paste is selected, and its properties are improved by powdered waste addition.

Firstly, the physico-chemical mechanisms generating expansion in stoichiometric MKPC paste are analyzed. Swelling is attributed to a pH gradient in the paste, due to the progressive sedimentation of MgO particles in the fresh mix.

Secondly, over-stoichiometric MgO is replaced by varying amounts of minerals simulating the waste, of different mineralogy and granulometry, in order to achieve sufficient workability and no swelling. An optimal formulation is proposed, which incorporates powdered fly ash at a fine-to-cement mass ratio (F/C) of 1. Its mechanical performance and endogenous dimensional changes are comparable to typical over-stoichiometric pastes, and they stabilize between 7 to 28 days.

© 2020 published by Elsevier. This manuscript is made available under the CC BY NC user license
https://creativecommons.org/licenses/by-nc/4.0/

Keywords: Magnesium potassium phosphate (MKP) cement; Magnesium-to-phosphate (Mg/PO_4) molar ratio; Fine to cement (F/C) mass ratio; Swelling inhibition; Hazardous waste immobilization

1. Introduction

1.1- Industrial background

In the nuclear energy industry, cementation is a promising way for the immobilization of hazardous waste, by both chemical stabilization and physical blocking processes [1]. However, Ordinary Portland Cement (OPC)-based materials are not systematically adapted for immobilizing nuclear waste, *e.g.* when significant corrosion reactions or swelling phenomena of the waste may occur, as with Mg/Zr alloys (used for uranium fuel cladding), aluminium powders, or plutonium waste sludge [2][3][4].

Although their carbon footprint remains relatively high [5], magnesium phosphate cements (MPC) are of primary interest to address these concerns. The pH of their pore water is generally comprised between 4 and 8 [6]; this inhibits corrosion mechanisms, e.g. when in contact with aluminium waste; alternately, chemical reactions with the phosphate precursor may be expected with some waste types. They are acid-base inorganic binders, resulting from the chemical reaction between an alkaline magnesia source and a phosphate acid source. The first developed MPC were based on ammonium dihydrogen phosphate ($NH_4H_2PO_4$) as an acid source [7][8][9]. However, their applicability is limited, because ammonia gas (NH_3) is released during the setting process. Since then, other acidic sources have been proposed to avoid this issue.

Monopotassium dihydrogen phosphate KH_2PO_4 is the most widely used acid for MPC preparation. The resulting cement is called Magnesium Potassium Phosphate Cement (MKPC). MKPCs display fast setting time, high compressive strength at early age and good chemical stability [10] [11] [12]. These characteristics make it a material of choice for road repairs and for solidification/stabilization of radioactive materials [4][13].

1.2- Scientific context

The final stoichiometric reaction product in MKPC is a magnesium potassium phosphate hexahydrate (struvite-K, $MgKPO_4.6H_2O$) [6]. The whole MKPC setting process is summarized by the following *global* chemical reaction:

$$MgO + KH_2PO_4 + 5\,H_2O \rightarrow MgKPO_4.6H_2O \quad (1)$$

It is characterized by a magnesium-to-phosphate molar ratio Mg/PO_4 *i.e.* (Mg/P) equal to 1, and a water-to-cement mass ratio (W/C) of 0.51 (where cement C corresponds to both MgO and KH_2PO_4). However, stoichiometric MKPC displays significant volume changes (expansion) after setting [14] [15]. This requires precautions when developing MKPC formulations, generally by adding over-stoichiometric MgO. Le Rouzic *et al.* [15] and Xu *et al.* [16] show that the swelling of MKPC paste disappears for (Mg/P) > 3. According to Xu *et al.* [14], the optimal (Mg/P), which avoids swelling and provides optimal mechanical performance, is of between 6 and 8. This provides compressive strength of up to 65 MPa after 200 days maturation.

Different reaction mechanisms, leading to struvite-K, have been proposed in the literature [7] [6] [17] [18]. They mainly depend on (Mg/P) and (W/C). Swelling is explained by the formation of expanding intermediate phases, due to chemical reactions occurring before struvite-K is formed [19]. Qiao [17] suggests a mechanism in five successive stages, based on successive dissolution and precipitation phenomena, for pH values ≥ 6.3. In particular, these chemical reactions lead to phosphorrösslerite $MgHPO_4.7H_2O$ and to a magnesium potassium phosphate hydrate $Mg_2KH(PO_4)_2.15H_2O$. Complementarily, Le Rouzic *et al.* [20] show the formation of newberyite $MgHPO_4.3H_2O$ as another intermediate phase towards the formation of struvite-K, at a pH lower than 6. By using diluted MKPC mixes, Lahalle *et al.* [21][22] show an increase in the diversity of intermediate hydrate phases when decreasing the (W/C) ratio. The (Mg/P) ratio also has a significant impact on volume changes. Indeed, with a

greater amount of available MgO, acid-base reactions are accelerated. This prevents the formation of intermediate hydrates and limits swelling [16].

An alternative route to reduce swelling consists in replacing over-stoichiometric MgO by other minerals, e.g. fly ash FA [3,11,12,23–25], ground granulated blast furnace slag GGBFS [6,26,27] or silica fume SF [28]. This allows to decrease the proportion of MgO in the cement down to values close to stoichiometry, with Mg/P ratios of 0.8 [29], 1 [3] [23], or 1.7 [26]. In such instance, keeping the MgO content at a low value also avoids the formation of highly expansive brushite $Mg(OH)_2$ on the long term [16], and limits the cost and carbon footprint of MKPC. FA and GGBFS have physical effects on MKPC. By diluting the cement matrix volume and decreasing the heat release during cement setting, FA and GGBFS are recognized as setting retarders; FA increases the paste fluidity in the fresh state, improves mechanical strength and water resistance, and reduces drying shrinkage [12,29].

Although FA, GGBFS and SF are generally considered as inert minerals in over-stoichiometric MKPC matrices [30], some interactions have been evidenced. In particular, for MKPC added with low Ca content FA (i.e. Class F FA), at a low (Mg/P) ratio of 1.7, Gardner et al. [26] show the formation of an amorphous aluminium phosphate phase; a similar amorphous product is observed for MKPC added with GGBFS. Interactions are also noted with high Ca content FA (i.e. Class C FA), see for instance [30]. However, when mixing Class C FA and KH_2PO_4, a high content in KH_2PO_4 is required to provide reaction products; the mechanical strength of these products is of only about 10 MPa at 28 days [31], whereas up to 60 MPa are achievable at 28 days with struvite-K [16]. Therefore, when mixing both FA and MgO with KH_2PO_4 to manufacture a MKPC, competing acid-base reactions are expected (FA + KH_2PO_4 simultaneously to MgO + KH_2PO_4). The resulting material may not have optimal mechanical performance if FA reacts with KH_2PO_4.

In the case of SF, authors generally agree that the solubility of Si is low at near neutral pH [26], so that SF is still considered an inert mineral in MKPC.

1.3- Aims and scopes

This research aims to recycle finely divided industrial waste (and ultimately, hazardous or radioactive ones) into MKPC. The targeted waste powders are of micrometric size.

In this contribution, the waste is replaced by SF, Class F FA or quartzitic sand, spanning a similar granulometry range. To our knowledge, there is currently no systematic study on the effect of fine mineral additions on a stoichiometric MKPC matrix, neither for understanding the mechanisms avoiding swelling, nor for optimizing its content for industrial purposes.

Our global approach is described in **Fig. 1**. The first part aims to understand the mechanisms at the origin of volume changes in stoichiometric MKPC, and to contribute to their inhibition. This part combines Thermo-Gravimetric Analysis coupled to Differential Thermal Analysis (TGA-DTA) and X Ray Diffraction (XRD). Stokes' law for calculating the sedimentation rate is also used to interpret the observations.

Secondly, swelling is avoided by adding different granular minerals, with varying nature, granulometry and amount. The introduced minerals (quartzitic sand, fly ash FA and silica fume SF) are surrogates of actual hazardous waste. Particular care is taken to achieve an optimal MKPC paste with sufficient workability and compressive strength. The hydrate products are analysed by TGA-DTA and XRD in order to determine potential interactions between the introduced minerals and the MKP cement.

Finally, for the optimal formulation based on FA, the homogeneity, mineralogical composition and bond strength of the FA particles-MKPC paste are investigated by Scanning Electron Microscopy (SEM). Due to a high content in paramagnetic matter, NMR did not yield adequate results. Instead, Fourier Transform InfraRed spectroscopy (FTIR) is used to

determine whether products due to FA reacting with KH_2PO_4 are present. Comparison is done with over-stoichiometric MKPC (made with excess MgO and no FA).

2. Materials and methods

2.1. Raw materials

MKPC pastes are prepared using hardburnt MgO (Magchem 10 CR from M.A.F. Magnesite BV, purity 98.3%), potassium dihydrogen phosphate KH_2PO_4 (purity 99% from Acros Organics) and deionized water, as in [3]. The mineral additions used in replacement to over-stoichiometric MgO are class F Fly Ash (FA) from a local thermal power station (Harnes, France), commercial densified silica fume (SF) and pure quartzitic (silica) sand (Société Nouvelle du Littoral, Leucate, France).

The powders are characterized by X-Ray Fluorescence (XRF), with a Bruker© S2 Ranger apparatus, equipped with a palladium tube. The specific surface area of the particles is determined by gas sorption, with the BET method, with a FlowSorb II apparatus from Micromeritics©. The analysis gas is a mixture of nitrogen and helium at 30%mol. For all powders, chemical composition, BET specific surface area and absolute density (measured by helium pycnometry) are described in **Table 1**. A very small amount of a mineral phase containing magnesium (2.90%wt of MgO) is present in FA, but it may not be available to form a magnesium-phosphate cement; otherwise, its CaO content classifies this FA as a class F (low Ca content) FA. SF has a significantly greater specific surface area than FA, which is bound to affect paste workability to a larger extent than FA.

The particle size distribution (PSD) of MgO and KH_2PO_4 is determined by laser granulometry with a MASTERSIZER 3000 (Malvern Panalytical, UK), using a liquid dispersant (water for MgO and ethanol for KH_2PO_4). Due to the agglomeration of fly ash and silica fume powder particles with laser granulometry, their PSD is determined using a digital optical microscope,

a MORPHOLOGI G3 (Malvern Panalytical, UK). In this case, powder dispersion is carried out using a SDU (sample dispersion unit), with a powder amount of 1 mm^3, a dispersion argon gas pressure of 300kPa, and a deposition time of 1 minute. Each particle is digitized and its morphology (particle size and shape) is measured.

Fig. 2a shows that the grain size range of MgO is greater than FA. Comparatively, SF is significantly finer than both MgO and FA (with a d_{50} smaller than one micron), see also **Figs. 2b and c**. Silica sand is used by selecting individually five different granulometric classes (80-160µm; 160-315 µm; 315-630 µm; 630 µm-1.25 mm and 1.25-2.50 mm). All of these sand classes are significantly bigger than MgO, but the whole sand granulometry (compliant with the EN 196-1 standard) is close to that of KH_2PO_4.

Compared to Cau-Dit-Coumes *et al.* [3], the FA used in this study is finer (with d_{10}=1.50 µm, d_{50}=5.75 µm and d_{90}=12.40 µm here, compared to d_{10} = 3 µm, d_{50} = 24.2 µm and d_{90}=136.1 µm in [3]); it also has a different chemical composition (with more Fe_2O_3, slightly more CaO, less SiO_2 and Al_2O_3). The FA used in this research is closer to those in Gardner *et al.* [24] in terms of granulometry and specific surface area S_{BET}.

2.2. Paste formulations

All formulations are summarized in **Table 2**, with their associated analysis means. In order to prevent the MKPC from setting too quickly, boric acid H_3BO_3 is added in all formulations at 3%mass cement, as in [32]. For a better understanding, in all formulation labels, M represents the molar ratio (Mg/P) times 100 and W the water-to-cement mass ratio (W/C) times 100.

Stoichiometric MKPC (**M1W51-Mg**) is made to understand swelling mechanisms. The latter is inhibited using varying amounts of SF, FA (with a Fine-to-Cement ratio F/C ranging between 0.05 to 1.4) or silica sand (with a Sand-to-Cement ratio S/C ranging between 0.5 and 3).

For chemical and structure analysis, the optimal MKPC pastes made with FA or SF at a fine-to-cement mass ratio F/C of 1 (**M1W51FA1** and **M1W51SF1**) are compared to an over-stoichiometric MKPC paste made with the same F/C and W/P but using MgO instead of FA or SF, i.e. with a Mg/P=5.39 and W/P=W/C= 0.255 (**M5.39W25.5**). They are also compared with the optimal MKPC paste in terms of compressive strength, at Mg/P=6 and W/P= 0.20 (**M6W20**).

For comparing mechanical performances, the optimal stoichiometric paste incorporating FA **M1W51FA1** is compared to the over-stoichiometric MKPC paste at a Mg/P of 6 and W/C=0.20 (**M6W20**). Indeed, by varying Mg/P between 4 and 6 and W/C between 0.2-0.3, preliminary research [33] has shown that Mg/P=6 and W/C=0.2 are the optimal values for maximizing the uniaxial compressive strength at 28 days in over-stoichiometric MKPC pastes, instead of **M5.39W25.5**, when using the raw materials described above.

For more details on the mix design, **Table 3** provides the weight composition of the main MKPC pastes of this research.

2.3. Mixing and curing protocols

All pastes are manufactured according to the 4 minutes mixing protocol described in the EN 196-1 standard. Preliminarily to mixing, boric acid is dissolved in water.

Once the pastes and mortars are made, their rheology is characterized with a mini-slump test (see below). After this measurement, the pastes are cast in tubes of 2.5 cm diameter and 6 cm height for volume change measurement. Lateral deformations are hindered by using thick rigid tubes, so that only longitudinal (vertical) deformations are permitted.

For mechanical and length change testing, pastes are poured in 4x4x16 cm^3 moulds, and sealed in airtight containers. For compressive strength, samples are cut in two 4x4x4cm^3 cubes by a three point bending test at the desired curing duration. Prior to testing, all samples

are sealed and matured at 20°C in a temperature-controlled room for 1, 7 or 28 days (endogenous curing).

2.4. Charaterization methods

2.4.1. Chemical characterization

These methods are used for the two parts of the research, first for understanding swelling mechanisms, and secondly for optimizing a MKPC cement incorporating powdered minerals.

ThermoGravimetry Analysis – Differential Thermal Analysis (TGA-DTA). After 7 days endogenous curing of different MKPC pastes, TGA-DTA is performed on small sized-samples (obtained by saw cutting bigger samples and powdering them with a mortar and pestle), from room temperature to a target temperature of 700°C, at a slow heating rate of 5°C per minute, under an argon atmosphere. The device used is a SETARAM© differential thermal analyser, providing both sample mass and heatflow (in micro-volts) over time. Phase decomposition temperatures are determined by deriving the mass signal over time. All specimens are tested directly according to schedule in order to avoid hydration stopping operations.

Qualitative X-Ray Diffraction (XRD). After 7 or 28 days of endogenous curing, MKPC paste samples are hand ground (with a mortar and pestle) and characterized with a BRUKER© D8 advance apparatus (Cu Kα radiation), with a 2θ angle between 5° and 60°, at a step of 0.02°, and an analysis time of 1 second. All specimens are tested directly according to schedule in order to avoid hydration stopping operations. Phase identification uses the ICSD database and the DIFFRAC.EVA software (BRUKER©).

FTIR (Fourier Transform InfraRed) analysis. FTIR spectra are measured over the wavenumber range 4000 - 400 cm^{-1} using a Perkin Elmer Spectrum Two™ apparatus equipped with a diamond attenuated total reflectance system. Each monolithic sample is characterized at room temperature, and the number of scans (to decrease the signal-to-noise ratio) is set to 10. The 1200-600 cm^{-1} wavenumber range is presented only, because it is where phosphate vibrations are visible. After 28 days of endogenous curing, the stoichiometric matrix **M1W51FA1** made with FA is compared with pure minerals and intermediate phases. The latter are $MgHPO_4.3H_2O$, $MgHPO_4.7H_2O$, $Mg_2KH(PO_4)_2.15H_2O$ and struvite-K. For FTIR analysis, they are synthesized following the protocols presented in [34,35]. The purity of each solid is verified by XRD.

Scanning Electron Microscopy (SEM) analysis. SEM observations are performed with a JEOL JSM-7800F apparatus equipped with secondary electron (SE) and backscattered electron (BSE) detectors, operated at a 15kV acceleration voltage and at a working distance of 8.5 mm +/-0.1 (or 10 mm+/-0.1 for EDX mapping). After 28 days curing, the **M1W51FA1** paste is impregnated with epoxy resin, surface-polished with abrasive disks and gold-coated. Elemental cartography is performed using an Energy Dispersive X-ray (EDX) detector (Oxford Instruments, UK) with a minimal photon count number (more than 10,000). Alternately, after 28 days endogenous curing, fracture surfaces of **M6W20** and **M1W51FA1** pastes are gold-coated and observed for analysis of the failure facies.

2.4.2. Rheological behaviour

An important rheological parameter for cement pastes is their workability, *i.e.* the fluidity of the paste. The easiest way to measure it by using the slump cone test. This method provides the subsidence or the spread of the paste. However, one of its major disadvantages is the

amount of paste needed, and therefore, the amount of raw material required. This is prohibitive with hazardous waste recycling, or for costly raw minerals such as MgO.

Extensive research has been conducted on the miniaturization of this test [36,37], see **Fig. S1 top**. For magnesium phosphate mortars, Li *et al.* [36] use an Abrams mini-cone with a 148.44 cm^3 volume (top diameter of 3 cm, bottom diameter of 6 cm and height of 9 cm). For alkali-activated fly ash pastes, Tan *et al* [37] show a good correlation between the slump cone test using a cone of 38.37 cm^3 volume, and tests conducted using a conventional blade viscometer. Their mini-cone is smaller than that in [36] by a factor of 1.56. The present study uses a similar cone for MKPC pastes, but with smaller dimensions than for both [36] and [37]. It is at an homothetical factor of 2.4 compared to the cone in [36]. Our Abrams mini-cone has dimensions of 1.25 cm top diameter, 2.5 cm bottom diameter and 3.75 cm height, corresponding to a volume of 10.75 cm^3.

In terms of experimental protocol, each workability test is made by preliminarily oiling the cone, and filling it with fresh paste (**Fig. S1 bottom**). To allow comparison between different formulations, a relative spread parameter S_r is defined. When the paste displays slump (stiff paste), S_r is taken equal to the ratio between the height of the demoulded paste and the height of the cone. When the paste displays spread (flowing paste), S_r is the ratio of between the spread diameter and the bottom cone diameter B_0. In case of spread, S_r is taken as the average of two measurements (two orthogonal diameters of the spread) per spread, and for each formulation, the spreading test is repeated three times (with different pastes).

2.4.3. Volume change measurement

This experiment aims at quantifying MKPC swelling, by determining the volume change of the paste after a given setting time. As described above, the paste is placed in a thick rigid 2.5 cm diameter tube. The initial paste height H_0 (at the time of its synthesis) is measured, and the tube is then sealed for 28 days (airtight curing). After these 28 days, sample height H_{28} is

measured between the top of the tube and the paste surface, with an accuracy of +/-0.5mm. The two H_0 and H_{28} values provide the percentage of volume change $\Delta H(\%)$ as:

$$\Delta H(\%) = \frac{H_{28} - H_0}{H_0} \times 100 \quad (2)$$

In practice, due to the tube stiffness, if a volume change occurs, its height only is affected. The value of ΔH corresponds to three distinct cases. If ΔH is negative, the sample has shrunk; if ΔH is positive, the sample has swollen. If ΔH is 0, the sample displays dimensional stability.

2.4.4. Setting time

The setting duration is measured using an automatic Vicat prisometer (E2ME, France) according to NF EN 196-3.

2.4.5. Mechanical performance

Uniaxial compressive tests are carried out on 4*4*4 cm^3 cubes, according to EN 196-1. The samples are tested at given endogenous curing times of 1, 7 and 28 days. For each formulation and curing time, 6 samples are tested until failure. Two formulations **M1W51FA1** (Mg/P=1, W/C=0.51, F/C=1) and **M6W20** (Mg/P=6, W/C=0.2) are characterized by this method.

2.4.6. Dimensional change measurement

Three specimens of the two optimal formulations (**M1W51FA1** and **M6W20**) are equipped with brass studs at both ends. Dimensional length change is measured as recommended by NF P15-433 and NF P18-427. Between each measurement, each specimen is covered with an aluminium adhesive film and subjected to endogenous curing in an airtight bag, in an air-conditioned room at 21±1°C.

3. Results and discussion

3.1. Understanding the swelling of stoichiometric MKPC paste

The stoichiometric **M1W51-Mg** paste displays an immediate bleeding after mixing, which prevents any measurement of paste rheology (**Fig. 3 left**). In addition, once placed in a mold, phase segregation appears and develops over time. Water is also present at the surface, but it is no longer measurable after 7 days curing. After a few minutes curing and up to 7 days (**Fig. 3 right**), visual observation shows the presence of three distinct solid layers, one at the bottom (presence of undissolved KH_2PO_4 particles), one in the middle, and one at the top (attributed to MgO particles). This is analyzed in more detail by XRD and TGA-DTA, by carefully taking off parts from each of the three solid layers.

3.1.1. Thermogravimetry (TGA-DTA)

For each of the three parts, the decomposition temperatures reveal a significant difference in phase composition (**Fig. 4**). The top part of the sample has a single endothermic peak at 104°C, corresponding to the decomposition of Struvite-K with the release of water. The intermediate part has two endothermic peaks at 80°C and 118°C, attributed in the literature [34] to a hydrated phase of formula $Mg_2KH(PO_4)_2.15H_2O$ for the first one, and to Phosphorrösslerite $MgHPO_4.7H_2O$ for the other one. The lower part of the sample is characterized by the presence of two endothermic peaks, a first one at 80°C and a second at 226°C. The first peak is attributed to the magnesium phosphate hydrate of formula $Mg_2KH(PO_4)_2.15H_2O$, also present in the middle part of the sample. The peak at 226°C is attributed to a phase change of KH_2PO_4, owing to the preliminary thermal analysis of the pure compound and to [38].

The presence of KH_2PO_4 at the sample bottom is explained by its limited solubility in water (it is of 250g/l at 25°C, see [39]), compared to the amount needed to respect the stoichiometry of MKPC (fixed at 1528g/l water, for Struvite-K formation).

3.1.2. XRD analysis

A more accurate XRD analysis of the species present (other than with TGA-DTA) is given in **Table 4** and **Fig. S2**. At the sample surface (top part), the presence of two crystalline phases, namely Struvite-K ($MgKPO_4.6H_2O$) and magnesium oxide MgO is confirmed. No characteristic diffraction peaks of KH_2PO_4 are detected.

In the middle part of the sample, a total of 6 phases is revealed, 5 of which are known from the literature. These are Struvite-K ($MgKPO_4.6H_2O$), Phosphorrösslerite $MgHPO_4.7H_2O$, $MgHPO_4.3H_2O$, $Mg_2KH(PO_4)_2.15H_2O$, KH_2PO_4 and an unidentified phase. This same phase is also present in the analysis of the lower phase. It is not identified precisely by TGA, because its decomposition peaks are probably superimposed to those already identified.

The lower part displays three main phases, including KH_2PO_4, and the lower part has higher intensity of KH_2PO_4 (at 2θ=23.7°) diffraction peaks than the two others, which are also present in the middle part.

3.1.3. Interpretation of the observed swelling

The analysis is illustrated in **Fig. 5 (I a-d)**. Initially, for the stoichiometric matrix (**M1W51-Mg**), the water volume is significantly bigger than the powders volume. Moreover, the amount of both KH_2PO_4 and MgO powders is greater than their solubility in water at 25°C (250g/l for KH_2PO_4 and 6,2 mg/l for MgO, see [39]). Being hardburnt, MgO also has a slow reaction rate. This explains that, just after mixing, although KH_2PO_4 and MgO dissolve, they remain in significant amounts as powders in the liquid.

Right after mixing, the dissolved reactants are uniformly distributed in the paste. They form Phosphorrösslerite all over the sample volume, at the surface of undissolved MgO particles, at a pH around 6-7, see references [16,17]. The formation of Newberyite $MgHPO_4.3H_2O$ before Phosphorrösslerite is also probable in the first few hours or days, but it is only detected in very minor proportions after 7 days, meaning that it has transformed significantly (**Table 4**). Despite that, the initial volume of powder solids is too small to avoid water bleeding, *i.e.* an observable amount of water is present above the mix (**Fig. 5.I.a**).

A few moments after mixing, while Phosphorrösslerite progressively forms in the liquid, the undissolved particles of KH_2PO_4, and MgO start to sediment. The larger undissolved particles of KH_2PO_4 settle faster than the smaller ones made of MgO (**Fig. 5.I.b**). This is consistent with XRD results, where MgO is mainly present in the top part of the sample, and KH_2PO_4 is rather in the middle and bottom (**Table 4**).

The sedimentation rate (or velocity) of the particles is calculated using Stockes' law, as:

$$v = \frac{2r^2 g \Delta(\rho)}{9\mu} \quad (4)$$

where v is the sedimentation velocity (in $m.s^{-1}$), r is the particle radius, g is gravitational acceleration (in $m.s^{-2}$); $\Delta(\rho)$ is the difference in apparent density between particle and fluid (in $kg.m^{-3}$) and μ is fluid viscosity (in Pa.s). The sedimentation velocities of MgO and KH_2PO_4

are described in **Fig. 6**. The correspondence with the main grain sizes of MgO and KH_2PO_4 (determined by laser granulometry) is also presented, allowing a comparison of the main actual sedimentation velocities. Results show that the sedimentation rate of MgO particles is much smaller than that of KH_2PO_4 particles, although the density of MgO is higher. This correlates well with XRD and TGA-DTA observations.

As a consequence, the larger amount of KH_2PO_4 at the sample bottom leads to a pH gradient (with a lower pH at the sample bottom) and also to a locally varying molar ratio Mg/P (with a lower Mg/P at the bottom and higher Mg/P at the top). Therefore, progressively, depending on the height considered in the sample, a threshold is reached, allowing the transformation of Phosphorrösslerite into $Mg_2KH(PO_4)_2.15H_2O$. This transformation induces a decrease in the volume of the solids on the order of 20% [16] (see also the cell volumes of the phases, in Å3, in **Table 4**), meaning that a contraction of the solids occurs where it is formed. With increasing pH, Struvite-K can form from $Mg_2KH(PO_4)_2.15H_2O$ (according to [17]), which causes a 6% decrease in the volume of the solids [16], and thus further contraction leading to cracking. This is observed in the middle part of the sample (**Figs. 3 and 5.I.c**).

All along the solidification process, while the pH remains below 7.4, Phosphorrösslerite forms, and since its volume is much larger than that of MgO and KH_2PO_4, the sample volume becomes larger than its initial value (in the liquid state).

Further, as soon as $Mg_2KH(PO_4)_2.15H_2O$ forms, and when the pH is of at least 7.3 [17], Struvite-K starts to solidify. Because of the differential sedimentation between KH_2PO_4 and MgO, this pH range is only reached in the top part of the sample, so that Struvite-K is only present there (**Table 4** and **Fig. 5.I.d**).

This analysis is consistent with the thermodynamic studies conducted by Lothenbach et al. [35]. The authors show that for pH values below 7, only precipitation of newberyite $MgHPO_4.3H_2O$ is expected, but for pH values slightly higher, the formation of

$Mg_2KH(PO_4)_2.15H_2O$, $Mg_3(PO_4)_2.4H_2O$ or $Mg_3(PO_4)_2.22H_2O$ occurs. For a pH higher than 8 and a high concentration of K, Struvite-K precipitation starts.

In this context, the use of over-stoichiometric MgO avoids sedimentation of particles, which is responsible for the swelling of stoichiometric MKPC. In sufficient amount, it may also control and regulate the pH above 7 (buffering effect), and provide phase homogeneity in the solid state; in such instance, Struvite-K forms faster than newberyite $MgHPO_4.3H_2O$ or any other hydrate [35].

3.2. Inhibition of swelling

When using over-stoichiometric MgO, swelling is eliminated [16]. This is attributed to a greater pH and to a greater Mg/P ratio in solution, but also to the elimination of particle sedimentation. Although the former are inherent to MgO addition, the latter is expected to be obtainable with other particle types.

3.2.1. Impact of sand addition on the stoichiometric matrix

A first investigation incorporates different granular classes of silica sand (80-160 µm; 160-315 µm; 315-630 µm; 630-1250 µm and 1.25-2.50 mm) into the stoichiometric matrix, at different sand to cement (S/C) mass ratios of 0.5, 1, 1.5, 2, 2.5 and 3 (**Table 5** and **Figure S3**). Results show that for low S/C ratios (0.5 and 1), there is no swelling inhibition, whatever the sand grain size class used; sand particles sediment at the bottom of the tube, and swelling appears above the sand, inside the entire volume available. For higher S/C mass ratios (1.5 to 3), only the smallest sand grain size classes (80-160µm and 160-315µm) inhibit swelling of the **M1W51-Mg** paste. These sand classes are suitable for replacing MgO in over-stoichiometric MKPC. However, in the following, this possibility has not been investigated further, because of the significant difference with the granulometry of the foreseen radioactive

hazardous waste to encapsulate (of micrometric order). For bigger sand classes, swelling is consistently visible and located at the sample bottom.

3.2.2. Impact of fine addition on the stoichiometric matrix

A second investigation uses significantly finer particles than sand (SF and FA). Dimensional variations values ΔH (after 28 days curing) are presented in **Fig. 7a** with the indication of swelling presence - in red (or not – in green).

Swelling decreases when increasing the fine-to-cement (F/C) mass ratio. The elimination of swelling is obtained at a minimal (F/C) of 0.6 for SF, and 0.8 for FA. For greater (F/C) than these values, no swelling is observed; this is consistent with the results of Cau-dit-Coumes et al. performed at (F/C)=1 [3]. The remaining effect of the additional powders is solely on paste rheology, see **Fig. 7b**. With SF, the rheology is not sufficient (no spread is achieved for reasonable F/C values), contrarily to FA. For (Mg/P)=1.7, with FA addition, Gardner et al. [24] also show good spread and swelling inhibition.

Complementarily, in **Fig. 7a**, the water-to-powder volume ratio V_W/V_P is plotted as a function of (F/C), for both FA- or SF-added MKPC. All formulations being made at a constant water proportion (W/C=0.51), the V_W/V_P ratio decreases with increasing (F/C) ratio. For a value $V_W/V_P = 0.6$ and below, swelling is avoided, i.e. particle segregation is avoided. For (F/C) = 1, $(V_W/V_P) = 0.57$, i.e. the MKPC paste displays no swelling.

Understanding of swelling inhibition. The addition of FA or SF avoids phase segregation and also powder sedimentation. This allows a homogeneity of all the constituents of the MKPC paste. Therefore, KH_2PO_4 particles are better distributed inside the material after the mixing step, preventing the formation of a pH gradient (**Fig. 5 (II a-d)**). Struvite-K can be generated progressively and homogeneously in the whole volume.

3.2.3. Chemical analysis

Role of FA and SF additions in the stoichiometric MKPC.

As shown by the literature analysis, FA (and SF) could react in a MKPC matrix and form reaction products, possibly aluminum phosphates [26]. **Fig. 8** provides the raw XRD spectra of the initial reactive phases (KH_2PO_4, SF and MgO) and of over-stoichiometric **M5.39W25.5**, compared to **M1W51FA1** and **M1W51SF1** made with (respectively) FA and SF at a (F/C)=1.

As expected, SF and FA alone present an amorphous content, marked by a wide hump (centered around 22° for SF and 27° for FA); this feature remains visible in **M1W51SF1**, but it is less marked in **M1W51FA1**. Phase identification for **M5.39W25.5** only shows the presence of Struvite-K and remaining (over-stoichiometric) MgO.

For **M1W51SF1** and **M1W51FA1**, apart from inert phases present in SF or FA (Cristobalite or Mullite and Quartz), no intermediate hydrates are recorded. For both **M1W51SF1** and **M1W51FA1**, Struvite-K and MgO are the main phases present, meaning that the chemical reactions, leading to the formation of Struvite-K, are complete. Apart from that, no other crystalline phase is observed, and no new wide bump, typical of a new amorphous phase, is observed either.

This analysis is completed by the FTIR analysis of **M1W51FA1** cement in the range corresponding to phosphate phase vibrations (**Fig. 9**). Results are compared to pure phases (KH_2PO_4, intermediate phases and Struvite-K). **Figure S5** provides the XRD spectra of synthetized pure phases $MgHPO_4.3H_2O$, $Mg_2KH(PO_4)_2.15H_2O$ and Struvite-K. In the case of $MgHPO4.7H_2O$, no sufficient quantity of powder could be synthesized, so that the diffractogram has been deduced from the ICSD 107677 sheet.

In presence of FA, Si-O (and Si-O-Si…etc.) vibrations centered around 1000cm^{-1} exist, which will likely interfere with phosphate vibrational identification. However, this does not affect the phase assignments from FTIR.

The pure synthetized Struvite-K is characterized by the presence of a P-O stretching ν3(PO_4^{3-}) vibration at around 987 cm^{-1}. $MgHPO_4.3H_2O$ and $MgHPO4.7H_2O$ have several vibrational bands, including one around 1078 cm^{-1} corresponding to the vibration of HPO_4^{2-}, and a second vibrational band at 873 cm^{-1} (for PO_4^{3-} vibration). $Mg_2KH(PO_4)_2.15H_2O$ has a main vibration band around 1078 cm^{-1} and a secondary one around 987 cm^{-1}. KH_2PO_4 presents two types of vibrational bands, one at 1078 cm^{-1} corresponding to the vibration of HPO_4^{2-}, and a second vibrational band at 873 cm^{-1} (for PO_4^{3-} vibration).

M1W51FA1 is characterized by a main vibrational band at 987 cm^{-1}, which is attributed to the vibration of the PO_4^{3-} group of Struvite-K. Apart from this wide band, a very small one may be found at around 1078 cm^{-1} (possibly corresponding to traces of $Mg_2KH(PO_4)_2.15H_2O$), but no other phosphate phase vibration is present. The FTIR spectrum of **M1W51FA1** is almost identical to that of pure Struvite-K, although with different amplitudes. This analysis does not allow to distinguish any new phosphate phase, that interactions between FA and KH_2PO_4 could have generated.

It is concluded that for **M1W51FA1**, no significant interaction between FA and KH_2PO_4 is observed. On the basis of the XRD data, the same conclusion is yielded for **M1W51SF1**; no interaction between SF and KH_2PO_4 is observed. For both **M1W51FA1** and **M1W51SF1**, the pH is on the order of 7, which is bound to limit the dissolution rate of FA and SF. With these elements, in this research, both FA and SF are considered inert additions in stoichiometric MKPC.

Role of over-stoichiometric MgO in MKPC.

When using over-stoichiometric MgO, its role in the MKPC paste may be physical or chemical, i.e. it may act as a reactive or unreactive powder [16] [40].

The role of over-stoichiometric MgO in MKPC is determined by comparing three MKPC pastes, two using inert FA or SF (**M1W51FA1** and **M1W51SF1** respectively), and the third using MgO as a fine. In the last two formulations, an equivalent amount of MgO is determined by using the same volume as that of the fines introduced. This theoretical volume of MgO leads to an over-stoichiometric formulation with a molar ratio Mg/P of 5.39 (the so-called MgO-based MKPC referred to as **M5.39W25.5**), when the absolute density of FA and SF is taken at an average value of 2. The amount of water introduced is identical (W/P=0.255) in all three formulations. It is the amount required for a stoichiometric formulation with a molar ratio Mg/P of 1. These formulations are also compared to **M6W20**, because it is the formulation with over-stoichiometric MgO providing optimal mechanical performance, and it is close to formulation **M5.39W25.5**. **Table 6** shows the yields of the various compounds present in the MKPC pastes, as deduced from TGA-DTA. **Fig. S4** shows the corresponding TGA-DTA curves.

By considering a complete reaction of the raw mineral proportions into Struvite-K, the theoretical total mass loss is calculated at 20.3% for **M5.39W25.5** (with MgO) and also 20.3% for **M1W51FA1** and **M1W51SF1**. This means that with 16.6, 16.8 and 16.6% mass loss, **M5.39W25.5**, **M1W51FA1** and **M1W51SF1** are not fully transformed into Struvite-K. For both **M1W51FA1** and **M1W51SF1**, the total mass loss is of the same order of magnitude (i.e. between 16.8% and 16.6%).

These results mean that in MKPC paste, no retarding or accelerating effect of FA or SF is observed, when compared to over-stoichiometric MgO.

Nota: For **M6W20**, the yield in Struvite-K is of 88.6%, which is greater than the 81.8% measured for **M5.39W25.5**. This is explained in the literature by a greater amount in MgO

(which enhances Struvite-K formation) and a lower water content [16]. For both over-stoichiometric matrices, the hydration reactions leading to Struvite-K are not finished at 7 days, although they are advanced by 81.8 to 88.6%.

Setting of MKPC pastes. The setting duration is measured at a value of 25 mins (+/-2 mins) for the over-stoichiometric cement pastes **M5.39W25.5** and **M6W20** made with MgO only, whereas it is of 3h (+/-3 mins) for **M1W51FA1** and **M1W51SF1**. As expected [14,26,30], setting duration is significantly increased with the addition of FA or SF.

Partial conclusion. Finally, a (F/C) mass ratio of 1, associated to the stoichiometric MKPC paste added with FA, is chosen for further characterization (**M1W51FA1** formulation). With this value, the fine content is high, the paste spread and setting duration are suitable for the industrial application of stabilization and solidification of industrial waste, no undesirable phase (i.e. no chemically unstable phase) and no paste swelling are observed.

3.3. Characterization of an optimal formulation

The rheological and setting time measurements of fresh **M1W51FA1** paste have been presented earlier. Further characterization in the hardened state is provided below.

3.3.1. Microstructure analysis

SEM observations. The microstructure and elemental cartography (Mg, K, P and Al) of **M1W51FA1** paste are observed after 28 days on a polished surface (**Fig. 10**). The field of view is chosen in order to display a representative overview of the structure, i.e. FA particles and MKPC in sufficiently significant amount (with tens of FA particles). The observed microstructure is typical of the encapsulation of spheroidal FA in Struvite-K. FA particles are

best visible on Al cartography. Their spherical shape remains unchanged after 28 days in contact with the MKPC cement. Moreover, when superposing the P and Al cartographies, no significant overlapping is recorded at this observation scale. Again, this testifies of the absence of significant reactivity between FA and stoichiometric MKPC. The Mg cartography shows homogeneously distributed remnants of MgO. The K cartography is typical of a homogeneously distributed MKPC paste (where the K concentration is high- in green), and of homogeneously distributed FA spheres (where the K concentration is low – in dark).

Complementarily, fracture surfaces are also observed with the SEM, see **Fig. S6**. **Fig. S6a** shows a typical fracture surface of over-stoichiometric MKPC paste **M6W20**, without FA addition, whereas **Figs. S6b-d** show different areas in a **M1W51FA1** fractured sample.

In **Fig. S6b**, an apparent decohesion is observed at the interface between the Struvite-K cement and the FA spheres, meaning that the interface is weaker than the MKPC paste itself. This weak interface is not favourable to a good mechanical performance of the FA-MKPC mix. It is inferred that with silica sand or SF additions, the weakest areas would also be the interface between MKPC and the added mineral, due to the absence of significant chemical interactions; this means that mechanical performance is not enhanced either.

Fig. S6c show the typical brittle morphology of the failure surface of the MKPC cement. **Fig. S6d** displays the typical Struvite-K crystals, with FA cenospheres pushed at the crystal tips, in an open air-entrained pore. This testifies of the limited chemical affinity of FA for Struvite-K.

3.3.2. Mechanical performance

Results are summarized in **Table 7**. When comparing the **M1W51FA1** paste to the over-stoichiometric paste **M6W20** (made with MgO and no fines), similar compressive strength f_c is measured after 1 day curing (at 18 MPa), but a difference on the order of 15 MPa is obtained at 28 days. **M1W51FA1** is characterised by a compressive strength of 24.3±1.8 MPa at 28 days, and **M6W20** of 38.8±1.8 MPa at 28 days.

This phenomenon of reduced mechanical performance when FA is added has been pointed out earlier, e.g. by Li and Chen [12]. Indeed, the addition of FA or any other mineral additive causes a dilution effect of the Struvite-K cement [41][26]. Other research has been carried out on the substitution of over-stoichiometric MgO [29] by FA, showing that a maximum f_c of 66 MPa may be reached at 28 days by replacing 50% of the over-stoichiometric MgO with a (F/C)=0.55, when using Mg/P=8. This corresponds to a decrease in Mg/P from 8 to 4, i.e. a significant amount of over-stoichiometric MgO remains necessary. The biggest replacement percentage investigated in [29] corresponds to a Mg/P of 0.8 and a F/C of 1.74, but f_c is below 20 MPa at 28 days, i.e. it is significantly smaller than our optimal f_c value of 24.3 ± 1.8 MPa at 28 days with **M1W51FA1**.

3.3.3. Dimensional changes in endogenous conditions

Dimensional changes need to be anticipated for adequate structural design. The dimensional stability of **M6W20** and **M1W51FA1** is determined at up to 45 days (**Fig. 11).** For both formulations, sample mass loss is less than 1% at 28 days, due to the endogenous curing in an airtight bag.

The greatest increase in relative length change ε is measured for **M1W51FA1** between 1 and 45 days, with a maximum value of 1200 $\mu m.m^{-1}$ at 45 days. Xu et al. [16] have compared the volume change of two Mg/P molar ratios of 2.7 and 8. A difference of about 10 cm^3 per 100g of the initial paste is measured at 28 days between the two pastes. A Mg/P of 2.7 shows the largest volume increase of the MKPC paste, meaning that decreasing Mg/P favours dimensional changes.

After 45 days, expansion keeps progressing for both **M6W20** and **M1W51FA1** pastes; stabilization is expected over longer time durations, rather on the order of 300-400 days [16].

The measurements provided here for **M1W51FA1** are however relatively limited and comparable to other MKPC cured in different conditions [16].

4. Conclusion

Our study has investigated the origin of swelling of stoichiometric MKPC, and how to inhibit such phenomenon using mineral additions (quartzitic sand, FA or SF). The aim is to incorporate finely divided powdered waste into MKPC, by remaining with a low MgO content, i.e. by remaining with MgO at stoichiometry, in order to avoid forming brushite ($Mg(OH)_2$) [16], to limit the MKPC carbon footprint and the material cost. The performance of the optimal formulations is characterized in the fresh and hardened states. Potential interactions between fine minerals and MKPC are addressed.

The following conclusions are drawn:

- The swelling of stoichiometric MKPC results from the creation of a pH gradient in the material due to the sedimentation of KH_2PO_4 grains, which leads to the preferential formation of intermediate phases (mainly $MgHPO_4.7H_2O$ and $Mg_2KH(PO_4)_2.15H_2O$ at 7 days) depending on the pH value. The presence of these phases is observed in all the analyses carried out.
- Swelling inhibition of the stoichiometric MKPC paste is achieved with mineral additives. Two parameters are essential, which are the size of the particles used and their amount. With quartzitic sand, the use of a small grain size (160 microns and below) and a high S/C mass ratio (1.5 and more) inhibits swelling. With FA or SF, a minimal (F/C) mass ratio of 1, and more precisely, a water-to-powder volume ratio V_w/V_p lower than 0.60 avoids particle segregation.
- With FA at (F/C) = 1 in the stoichiometric MKPC (formulation **M1W51FA1**), a homogeneous distribution of the constituents is obtained, which avoids sedimentation of KH_2PO_4 particles, and in a longer term, the formation of intermediate hydrates, which would cause swelling. TGA-DTA at 7 days shows the presence of Struvite-K and remnants of MgO only. No new phosphate phase is detected by TGA, XRD or FTIR after

7 days curing of the FA-MKPC stoichiometric matrix, meaning that the interactions between FA-stoichiometric MKPC are negligible. No retarding or accelerating effect of FA or SF is observed, when compared to over-stoichiometric MgO.

- The stoichiometric formulation **M1W51FA1** shows a limited expansion in endogenous conditions (compared to previous research on MKPC).
- Compressive test results provide reasonable mechanical performance in uniaxial compression (f_c = 24.3 ± 1.8 MPa on average at 28 days endogenous curing at 25°C) for the stoichiometric formulation **M1W51FA1**. These results are smaller than for an over-stoichiometric MgO matrix. Nevertheless, it reduces the amount of MgO required for the manufacture of a MKPC matrix, and prevents the possible formation of $Mg(OH)_2$ in the long term. The decrease in mechanical performance when adding FA is mainly due to a dilution phenomenon of Struvite-K and to de-cohesions at the fly ash-MKPC interface.

Acknowledgments

This work has been carried out in the framework of the Integrated Collaborative Research Laboratory LR4CU ORANO/CNRS – ENSCL – Univ-Lille. MDC acknowledges ORANO and Univ-Lille for financial support (PhD grant). The authors thank Ms. Laurence Burylo for technical assistance with powder X-ray analysis, and the Civil Engineering laboratory at Centrale Lille Institut for formulation, length change and mechanical characterization (Mr Th. Dubois).

References

[1] F. Bart, C. Cau-dit-coumes, F. Frizon, S. Lorente, Cement-Based Materials for Nuclear Waste Storage, 2013. https://doi.org/10.1007/978-1-4614-3445-0.

[2] A. Rooses, D. Lambertin, D. Chartier, F. Frizon, Galvanic corrosion of Mg–Zr fuel cladding and steel immobilized in Portland cement and geopolymer at early ages, J. Nucl. Mater. 435 (2013) 137–140. https://doi.org/10.1016/j.jnucmat.2012.12.030.

[3] C. Cau Dit Coumes, D. Lambertin, H. Lahalle, P. Antonucci, C. Cannes, S. Delpech, Selection of a mineral binder with potentialities for the stabilization/solidification of aluminum metal, J. Nucl. Mater. 453 (2014) 31–40. https://doi.org/10.1016/j.jnucmat.2014.06.032.

[4] K.A. Law, S. Parry, N.D. Bryan, S.L. Heath, S.M. Heald, D. Knight, L. O'brien, A.J. Fuller, W.R. Bower, G.T.W. Law, F.R. Livens, Plutonium migration during the leaching of cemented radioactive waste sludges, Geosci. 9 (2019). https://doi.org/10.3390/geosciences9010031.

[5] E. Gartner, T. Sui, Alternative cement clinkers, Cem. Concr. Res. 114 (2018) 27–39. https://doi.org/10.1016/j.cemconres.2017.02.002.

[6] S.A. Walling, J.L. Provis, Magnesia-Based Cements: A Journey of 150 Years, and Cements for the Future?, Chem. Rev. 116 (2016) 4170–4204. https://doi.org/10.1021/acs.chemrev.5b00463.

[7] E. Soudee, Liants phosphomagnésiens : mécanisme de prise et durabilité, 1999.

[8] S.S. Seehra, S. Gupta, S. Kumar, Rapid setting magnesium phosphate cement for quick repair of concrete pavements - characterisation and durability aspects,

Cem. Concr. Res. 23 (1993) 254–266. https://doi.org/10.1016/0008-8846(93)90090-V.

[9] Q. Yang, X. Wu, Factors influencing properties of phosphate cement-based binder for rapid repair of concrete, Cem. Concr. Res. 29 (1999) 389–396. https://doi.org/10.1016/S0008-8846(98)00230-0.

[10] C.K. Chau, F. Qiao, Z. Li, Microstructure of magnesium potassium phosphate cement, Constr. Build. Mater. 25 (2011) 2911–2917. https://doi.org/10.1016/j.conbuildmat.2010.12.035.

[11] F. Qiao, C.K. Chau, Z. Li, Property evaluation of magnesium phosphate cement mortar as patch repair material, Constr. Build. Mater. 24 (2010) 695–700. https://doi.org/10.1016/j.conbuildmat.2009.10.039.

[12] Y. Li, B. Chen, Factors that affect the properties of magnesium phosphate cement, Constr. Build. Mater. 47 (2013) 977–983. https://doi.org/10.1016/j.conbuildmat.2013.05.103.

[13] A.S. Wagh, S.Y. Jeong, D. Singh, High strength phosphate cement using industrial byproduct ashes, High Strength Concr. Proc. (1999) 542–553.

[14] B. Xu, B. Lothenbach, A. Leemann, F. Winnefeld, Reaction mechanism of magnesium potassium phosphate cement with high magnesium-to-phosphate ratio, Cem. Concr. Res. 108 (2018) 140–151. https://doi.org/10.1016/j.cemconres.2018.03.013.

[15] M. Le Rouzic, T. Chaussadent, L. Stefan, M. Saillio, On the influence of Mg/P ratio on the properties and durability of magnesium potassium phosphate cement pastes, Cem. Concr. Res. 96 (2017) 27–41.

https://doi.org/10.1016/j.cemconres.2017.02.033.

[16] B. Xu, F. Winnefeld, J. Kaufmann, B. Lothenbach, Influence of magnesium-to-phosphate ratio and water-to-cement ratio on hydration and properties of magnesium potassium phosphate cements, Cem. Concr. Res. 123 (2019) 105781. https://doi.org/10.1016/j.cemconres.2019.105781.

[17] F. Qiao, Reaction Mechanisms of Magnesium Potassium Phosphate Cement and its Application, 2010.

[18] A.S. Wagh, Chemically Bonded Phosphate Ceramics: Twenty-First Century Materials with Diverse Applications: Second Edition, 2016. https://doi.org/10.1016/C2014-0-02562-2.

[19] C.K. Chau, F. Qiao, L. Zongjin, Potentiometric Study of the Formation of Magnesium Potassium Phosphate Hexahydrate, J. Mater. Civ. Eng. (2012) 586–591.

[20] M. Le Rouzic, T. Chaussadent, G. Platret, L. Stefan, Mechanisms of k-struvite formation in magnesium phosphate cements, Cem. Concr. Res. 91 (2017) 117–122. https://doi.org/10.1016/j.cemconres.2016.11.008.

[21] H. Lahalle, C.C.D. Coumes, A. Mesbah, D. Lambertin, C. Cannes, S. Delpech, S. Gauffinet, Investigation of magnesium phosphate cement hydration in diluted suspension and its retardation by boric acid, Cem. Concr. Res. 87 (2016) 77–86. https://doi.org/10.1016/j.cemconres.2016.04.010.

[22] H. Lahalle, C. Cau Dit Coumes, C. Mercier, D. Lambertin, C. Cannes, S. Delpech, S. Gauffinet, Influence of the w/c ratio on the hydration process of a magnesium phosphate cement and on its retardation by boric acid, Cem. Concr.

Res. 109 (2018) 159–174. https://doi.org/10.1016/j.cemconres.2018.04.010.

[23] H. Lahalle, C. Patapy, M. Glid, G. Renaudin, M. Cyr, Microstructural evolution/durability of magnesium phosphate cement paste over time in neutral and basic environments, Cem. Concr. Res. 122 (2019) 42–58. https://doi.org/10.1016/j.cemconres.2019.04.011.

[24] L.J. Gardner, V. Lejeune, C.L. Corkhill, S.A. Bernal, J.L. Provis, M.C. Stennett, N.C. Hyatt, Evolution of phase assemblage of blended magnesium potassium phosphate cement binders at 200 and 1000°C, Adv. Appl. Ceram. 114 (2015) 386–392. https://doi.org/10.1179/1743676115Y.0000000064.

[25] A. Covill, N.C. Hyatt, J. Hill, N.C. Collier, Development of magnesium phosphate cements for encapsulation of radioactive waste, Adv. Appl. Ceram. 110 (2011) 151–156. https://doi.org/10.1179/1743676110Y.0000000008.

[26] L.J. Gardner, S.A. Bernal, S.A. Walling, C.L. Corkhill, J.L. Provis, N.C. Hyatt, Characterisation of magnesium potassium phosphate cements blended with fly ash and ground granulated blast furnace slag, Cem. Concr. Res. 74 (2015) 78–87. https://doi.org/10.1016/j.cemconres.2015.01.015.

[27] D. Singh, R. Ganga, J. Gaviria, Y. Yusufoglu, Secondary Waste Form Testing: Ceramicrete Phosphate Bonded Ceramics, 2011.

[28] D.D. Zheng, T. Ji, C.Q. Wang, C.J. Sun, X.J. Lin, K.M.A. Hossain, Effect of the combination of fly ash and silica fume on water resistance of Magnesium-Potassium Phosphate Cement, Constr. Build. Mater. 106 (2016) 415–421. https://doi.org/10.1016/j.conbuildmat.2015.12.085.

[29] B. Xu, B. Lothenbach, H. Ma, Properties of fly ash blended magnesium

potassium phosphate mortars: Effect of the ratio between fly ash and magnesia, Cem. Concr. Compos. 90 (2018) 169–177. https://doi.org/10.1016/j.cemconcomp.2018.04.002.

[30] B. Xu, H. Ma, H. Shao, Z. Li, B. Lothenbach, Influence of fly ash on compressive strength and micro-characteristics of magnesium potassium phosphate cement mortars, Cem. Concr. Res. 99 (2017) 86–94. https://doi.org/10.1016/j.cemconres.2017.05.008.

[31] M. Mahyar, S.T. Erdoğan, Phosphate-activated high-calcium fly ash acid-base cements, Cem. Concr. Compos. 63 (2015) 96–103. https://doi.org/10.1016/j.cemconcomp.2015.09.002.

[32] D.A. Hall, R. Stevens, B. El-Jazairi, The effect of retarders on the microstructure and mechanical properties of magnesia-phosphate cement mortar, Cem. Concr. Res. 31 (2001) 455–465. https://doi.org/10.1016/S0008-8846(00)00501-9.

[33] M. De Campos, Valorisation de matière faiblement radioactive comme réactif dans la synthèse de matrices cimentaires, Université de Lille, Thése, 2020.

[34] H. Lahalle, Conditionnement de l'aluminium métallique dans les ciments phospho-magnésiens, Université de Bourgogne Franche-Comté, Thése, 2016.

[35] B. Lothenbach, B. Xu, F. Winnefeld, Thermodynamic data for magnesium (potassium) phosphates, Appl. Geochemistry. 111 (2019). https://doi.org/10.1016/j.apgeochem.2019.104450.

[36] J. Li, W. Zhang, Y. Cao, Laboratory evaluation of magnesium phosphate cement paste and mortar for rapid repair of cement concrete pavement, Constr. Build. Mater. 58 (2014) 122–128. https://doi.org/10.1016/j.conbuildmat.2014.02.015.

[37] Z. Tan, S.A. Bernal, J.L. Provis, Reproducible mini-slump test procedure for measuring the yield stress of cementitious pastes, Mater. Struct. Constr. 50 (2017). https://doi.org/10.1617/s11527-017-1103-x.

[38] S. Vyazovkin, T.L. Ferrin, Thermomechanical study of the high temperature phase transition in KH 2 PO 4, Solid State Commun. 113 (2000) 627–631. https://doi.org/10.1016/S0038-1098(99)00547-5.

[39] D.R. Lide, Handbook of Chemistry and Physics 84th edition, 2003.

[40] B. Xu, H. Ma, Z. Li, Influence of magnesia-to-phosphate molar ratio on microstructures, mechanical properties and thermal conductivity of magnesium potassium phosphate cement paste with large water-to-solid ratio, Cem. Concr. Res. 68 (2015) 1–9. https://doi.org/10.1016/j.cemconres.2014.10.019.

[41] Y. Tan, H. Yu, Y. Li, W. Bi, X. Yao, The effect of slag on the properties of magnesium potassium phosphate cement, Constr. Build. Mater. 126 (2016) 313–320. https://doi.org/10.1016/j.conbuildmat.2016.09.041.

LIST OF TABLES

Table 1: *Minerals characterization: chemical composition from X Ray Fluorescence analysis, specific surface area S_{BET} (from nitrogen sorption) and absolute density.*

Materials	**Chemical composition (% weight)**									**S_{BET} ($m^2.g^{-1}$)**	**Absolute density ($g.cm^{-3}$)**
	SiO_2	**Al_2O_3**	**Fe_2O_3**	**K_2O**	**CaO**	**MgO**	**TiO_2**	**SO_3**	**P_2O_5**		
Magnesium oxide MgO	-	-	0.15	-	1.26	97.79	-	-	0.74	0.28	3.58
KH_2PO_4	-	-	-	44.81	-	-	-	-	55.12	-	2.34
Silica fume (SF)	94.86	0.44	0.18	1.48	1.17	0.30	-	0.90	-	21.37	2.24
Fly ash (FA)	43.25	20.37	**14.58**	7.86	**6.58**	2.90	2.04	1.02	-	4.70	1.76

Table 2: *Summary of all the MKPC formulations used and their associated analysis*

Aim	*Analysis*	*Name, composition*	*Varying parameters*
(1) Understanding of swelling	**TGA-TDA XRD**	**M1W51-Mg** (Mg/P = 1, W/C = 0.51, 3% of H_3BO_3 by weight of cement)	None
(2) Inhibition of swelling	**Volume change measurement and micro-slump test**	**Incorporation of different granular classes of sand M1W51-Sand** (Mg/P = 1, W/C = 0.51, 3% of H_3BO_3, S/C = 0 to 3)	Grain size of sand, mass ratio S/C
		Incorporation of fly ash, M1W51-FA (Mg/P = 1, W/C = 0.51 corresponding to a W/P = 0.21 to 0.42, 3% of H_3BO_3, F/C = 0.05 to 1.4)	Mass ratio F/C
		Incorporation of silica fume, M1W51-SF, (Mg/P = 1, W/C = 0.51 corresponding to a W/P = 0.25 to 0.49, 3% of H_3BO_3, F/C = 0.05 to 1)	Mass ratio F**/C**
	Chemical and structure analysis (TGA-DTA, XRD SEM, FTIR)	**Incorporation of fly ash, M1W51FA1** (Mg/P = 1, W/C = 0.51, 3% of H_3BO_3, F/C = 1)	None
		Incorporation of silica fume, M1W51SF1, (Mg/P = 1, W/C = 0.51, 3% of H_3BO_3, F/C = 1)	
		Over-stoichiometric matrix with MgO, M5.39W25.5 (Mg/P = 5,39, W/C = 0.255 and 3% of H_3BO_3)	
		Over-stoichiometric matrix with MgO, M6W20 (Mg/P = 6, W/C = 0.2 and 3% of H_3BO_3)	
	Mechanical strength, shrinkage measurement	**Incorporation of fly ash, M1W51FA1** (Mg/P = 1, W/C = 0.51, 3% of H_3BO_3, F/C = 1)	None
		Over-stoichiometric matrix with MgO, M6W20 (Mg/P = 6, W/C = 0.2 and 3% of H_3BO_3)	

Mg/P = MgO+KH_2PO_4 molar ratio; W/C = water to cement (cement = MgO + KH_2PO_4); W/P = water to powder ratio (powder = cement + mineral additives), S/C = sand to cement mass ratio; F/C = fine-to-cement mass ratio; %H_3BO_3 incorporation in %mass of cement

Table 3: *Detailed composition of the main formulations in this study*

Name	Formulation				Mass composition (in g for 100 g)				
	Mg/P	W/C	F/C	W/P	MgO	KH_2PO_4	H_2O	Fly ash/ Silica fume	H_3BO_3
M1W51-Mg	1	0.51	-	0.51	14.9	50.7	33.1	-	1.9
M1W51FA1	1	0.51	1	0.255	9.0	30.3	20	39.2 (FA)	1.2
M1W51SF1	1	0.51	1	0.255	9.0	30.3	20	39.2 (SF)	1.2
M5.39W25.5	5.39	0.255	-	0.255	48.3	30.3	20	-	1.2
M6W20	6	0.2	-	0.2	52	29.3	16.3	-	2.4

Table 4: *Summary of the XRD phase identification of the 3 parts of the stoichiometric matrix* ***M1W51-Mg*** at 7 days. *Label X corresponds to the certain presence of the phase and (*) to a minor phase presence (i.e. with small peak intensity).*

Phases	**Cell volume (Å^3) (crystal system; space group)**	**Top phase**	**Middle phase**	**Bottom phase**
MgO (ICSD 158103)	74.69 (cubic; F m -3 m)	X		(*)
KH_2PO_4 (ICSD 201374)	387.29 (tetragonal; I -4 2 d)		X	X
$MgHPO_4.7H_2O$ Phosphorrösslerite (ICSD 107677)	1879.52 (monoclinic; C 1 2/c 1)	(*)	(*)	(*)
$Mg_2KH(PO_4)_2.15H_2O$ (ICSD 32527)	503.67 (triclinic ; P -1)		X	X
$Mg_3(PO_4)_2.22H_2O$ (ICSD 100365)	666.57 (triclinic ; P -1)		X	X
$MgKPO_4.6H_2O$ Struvite-K (ICSD 5289)	473.36 (orthorhombic; P m n 21)	X		
$MgHPO_4.3H_2O$ Newberyite (ICSD 8228)	1091.11 (orthorhombic; P b c a)		(*)	(*)
Unidentified species	**-**		X	X

Table 5: *Summary of the swelling inhibition results obtained at 28 days by mixing a stoichiometric MKPC paste with different granulometric sand classes. (S) corresponds to swelling and (NS) to the absence of swelling.*

S/C	**Granular class of standard sand**				
	80 to 160 µm	**160 to 315 µm**	**315 to 630 µm**	**630 to 1250 µm**	**Greater than 1.25 mm**
0.5	S	S	S	S	S
1	S	S	S	S	S
1.5	NS	NS	S	S	S
2	NS	NS	S	S	S
2.5	NS	NS	S	S	S
3	NS	S	S	S	S

Table 6: *Results computed from TGA-DTA analysis: mass losses and % in struvite-K for MKPC matrices, depending on molar ratio Mg/P and on the fines used, after 7 days endogenous curing.*

Name	Theoretical mass loss assuming full struvite-K formation (20-700°C) (% total sample mass)	Experimental mass loss (20-700°C) (%)	Yield in Struvite-K (ratio experimental/theoretical mass loss) (%theoretical loss)
M5.39W25.5	20.31	16.6	81.8
M6W20	16.7	14.8	88.6
M1W51FA1	20.3	16.8	82.6
M1W51SF1	20.3	16.6	81.9

Table 7: *Uniaxial compressive strength results of* ***M1W51FA1*** *and* ***M6W20*** *after 1, 7 and 28 days endogenous curing.*

Name	Uniaxial Compressive Strength (MPa)		
	at 1 day	at 7 days	at 28 days
M1W51FA1	17.1 ± 0.7	22.2 ± 1.1	24.3 ± 1.8
M6W20	27.2 ± 2.6	37,4 ± 2.8	38.8 ± 1.8

LIST OF FIGURES

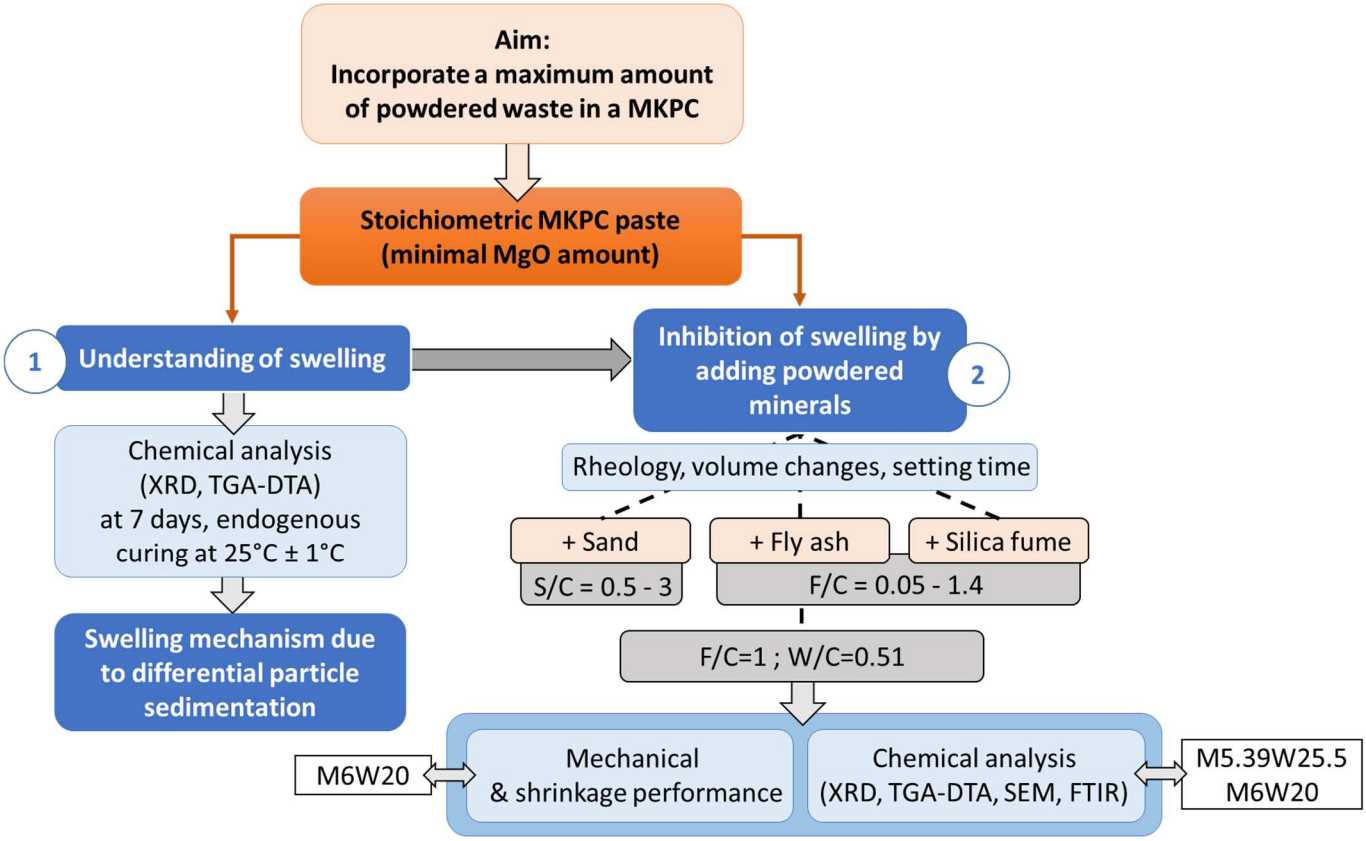

Figure 1: *Overview of the two-part experimental programme*

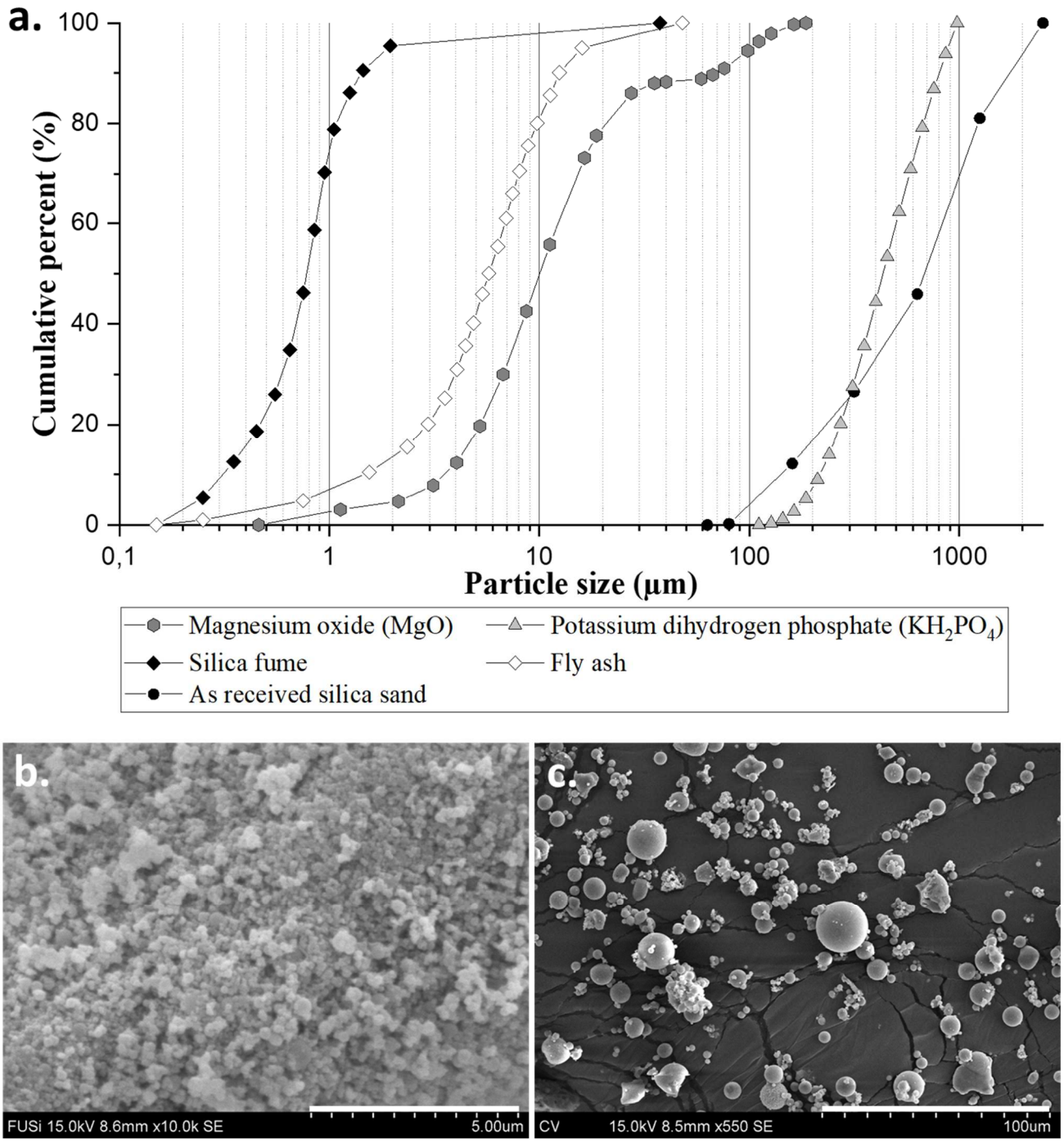

Figure 2: *(a.) Comparison of raw material granulometry measured by laser granulometry (for sand, MgO, KH_2PO_4) and morpho-granulometry (for silica fume and fly ash). Cumulative percentages are surface area proportions, i.e. they are similar to volume proportions; (b.) SEM photograph of silica fume SF (with a magnification x10,000, with the space between two successive scale bars representing 0.5 microns – and 5 microns for the whole scale), (c.) SEM photograph of class F fly ash FA (with a magnification x550, with the space between two successive scale bars representing 10 microns – and 100 microns for the whole scale).*

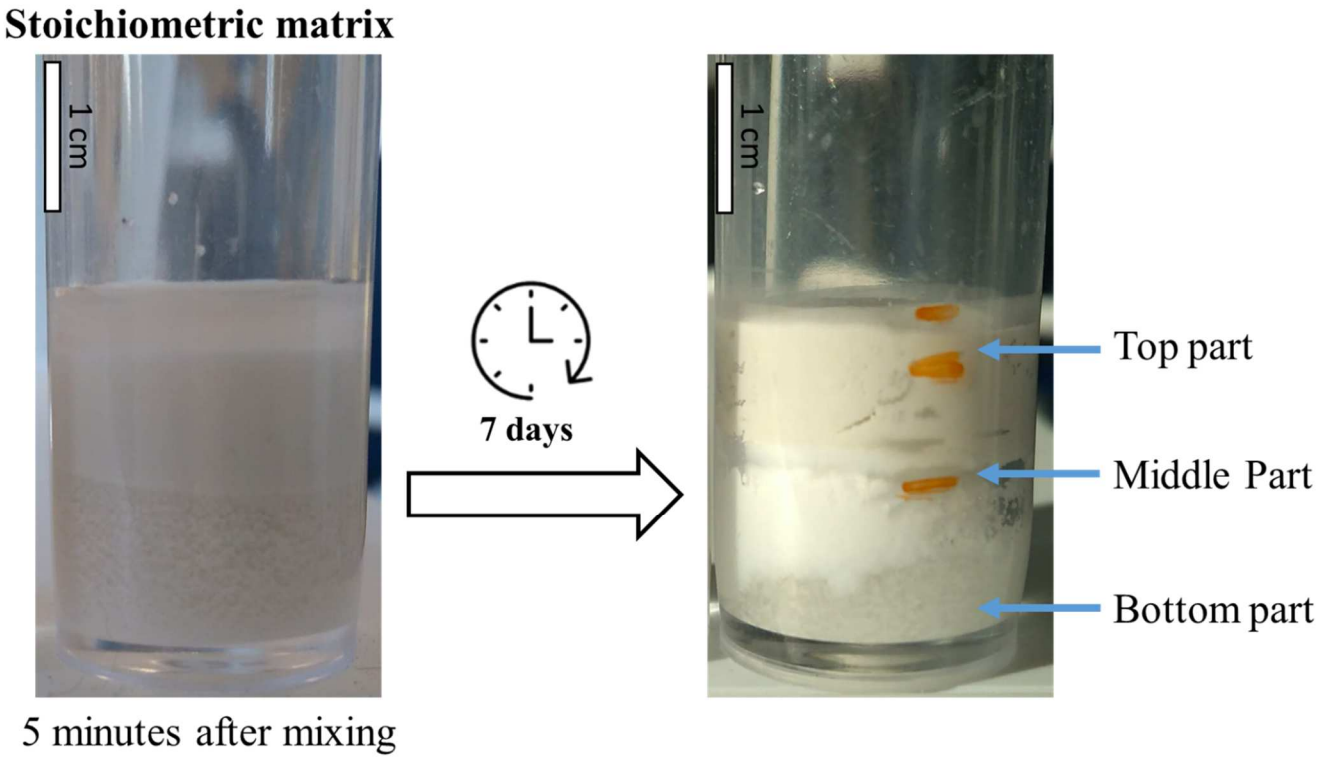

Figure 3: *Evolution of the* ***M1W51Mg*** *stoichiometric cement matrix, without fine addition, from 5 minutes after mixing (left) to seven days cure (right). Three distinct parts (bottom, middle and top) are observed.*

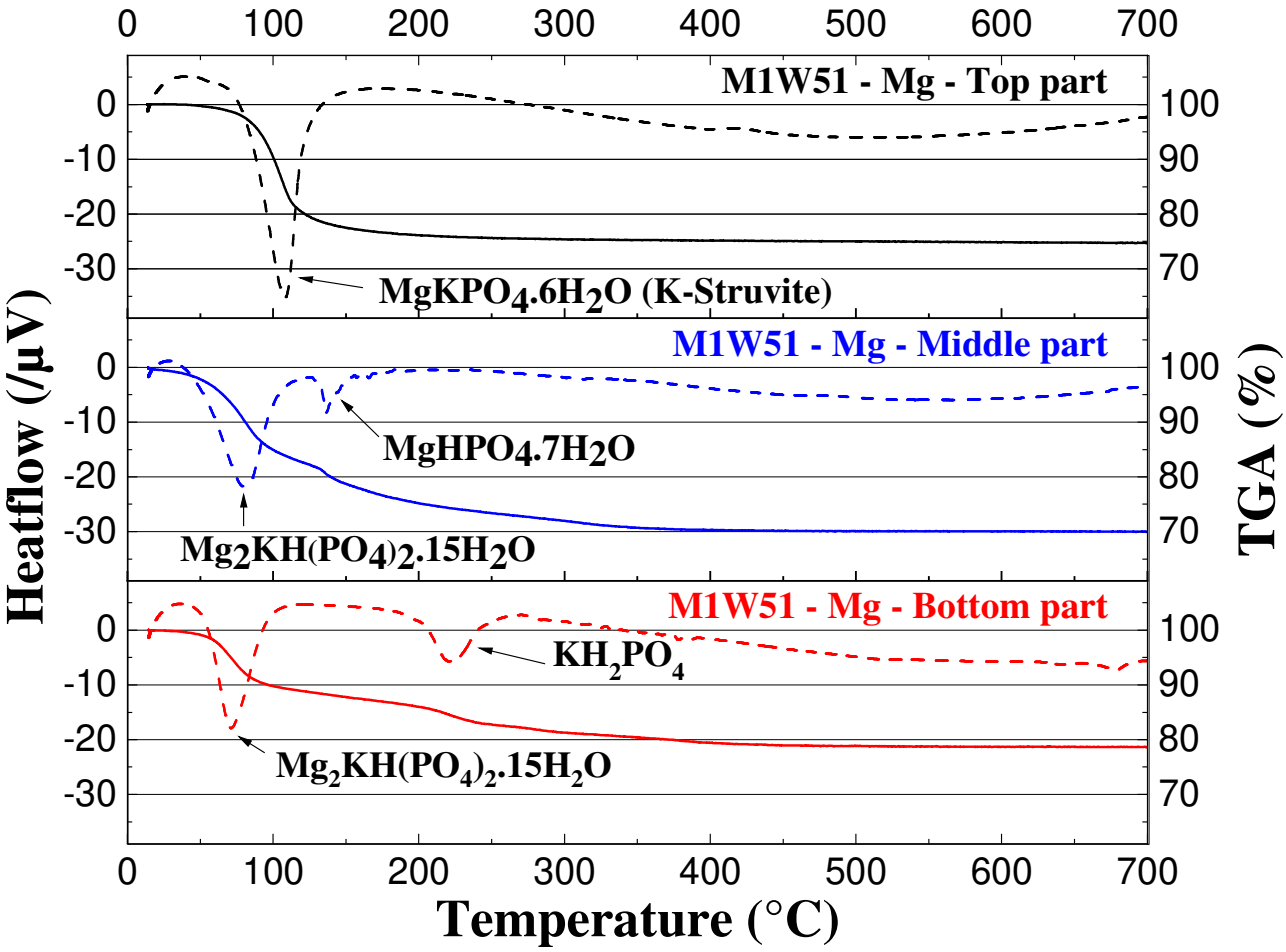

Figure 4: *TGA-DTA analysis for the 3 parts of the* ***M1W51-Mg*** *stoichiometric cement paste after 7 days endogenous curing.*

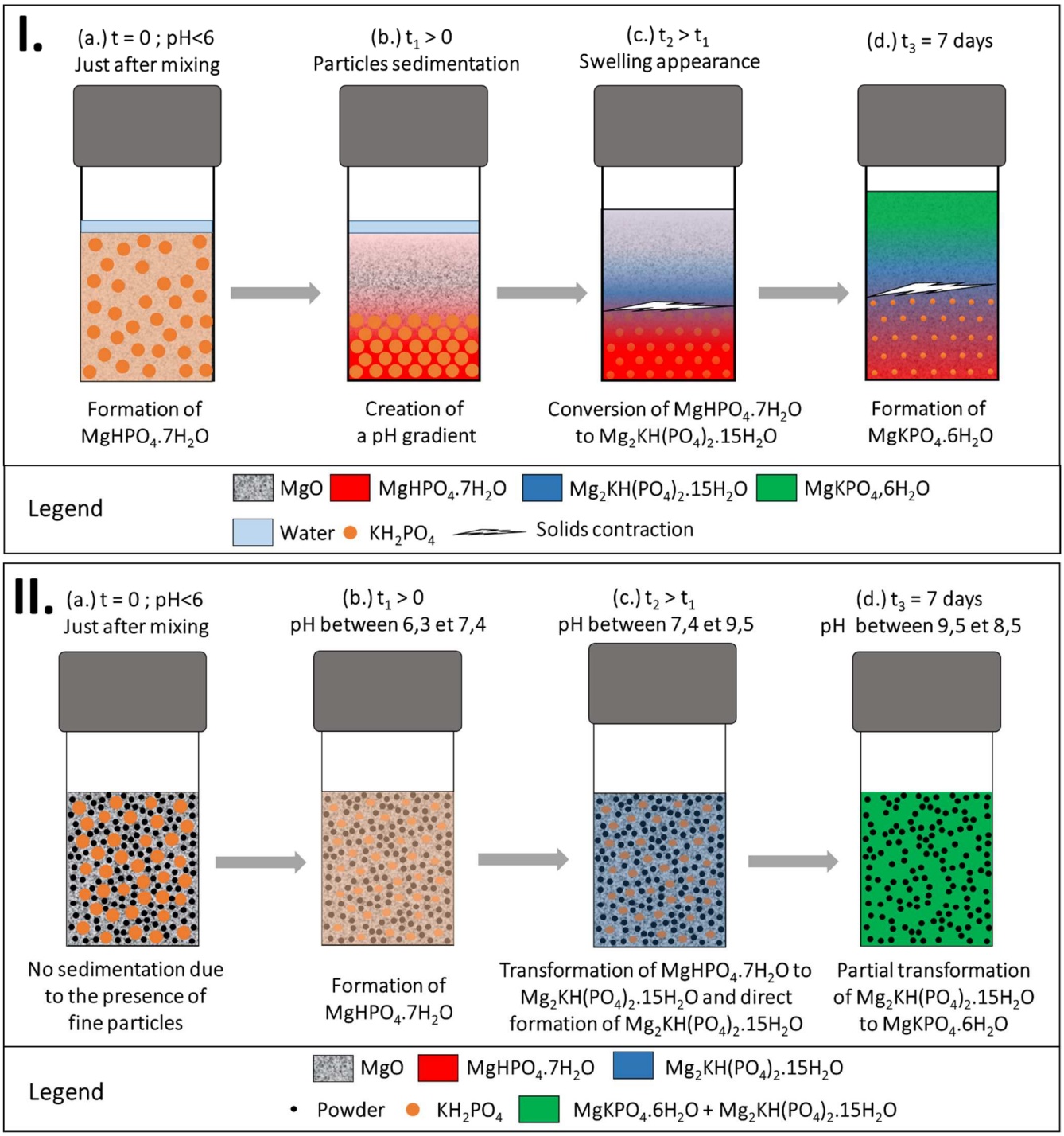

Figure 5: *Schematic mechanism of (I.) swelling development in the stoichiometric matrix (**M1W51-Mg**) and (II.) setting of the stoichiometric matrix with fine addition (e.g. **M1W51FA1** or **M1W51SF1**).*

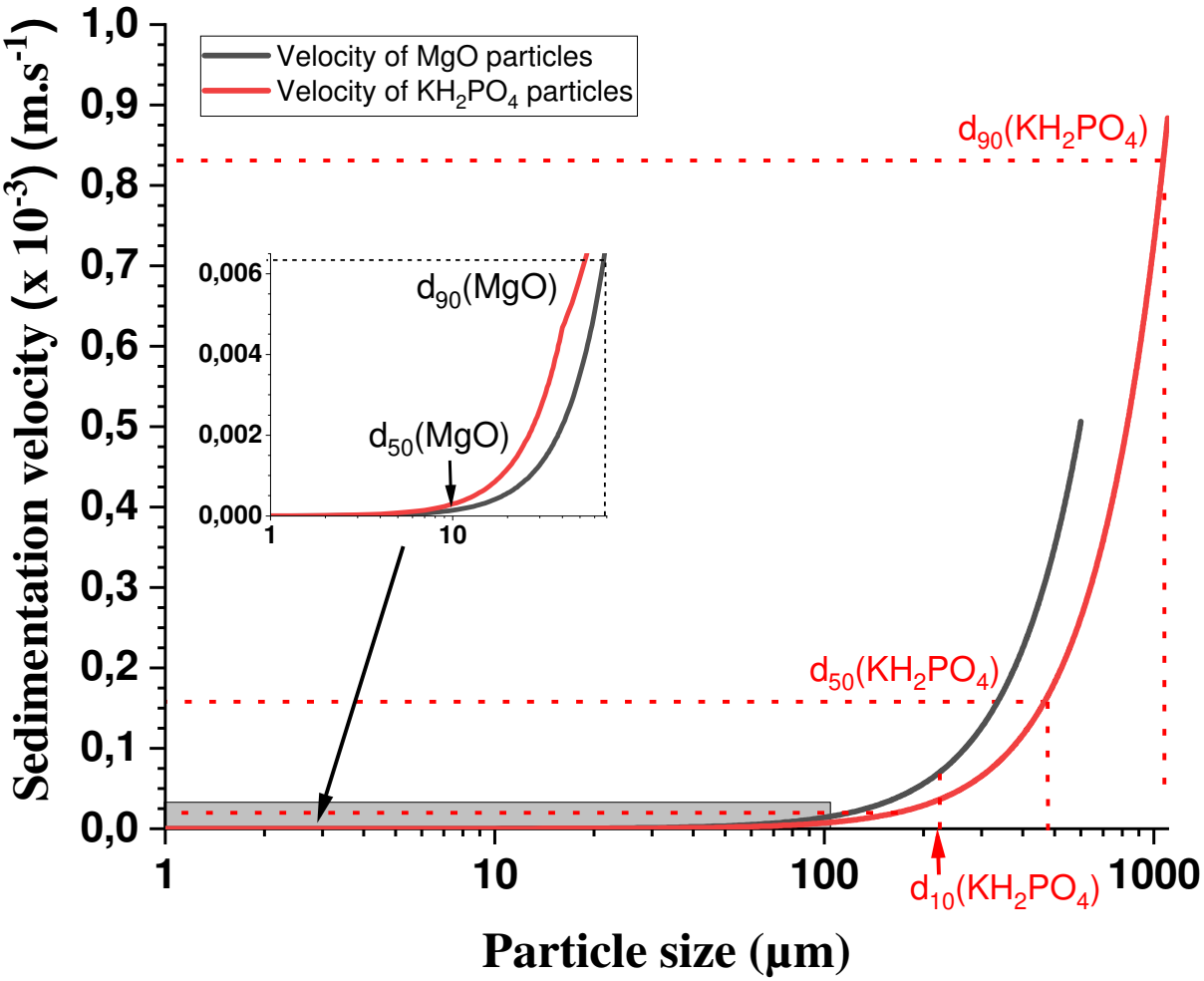

Figure 6: *Evolution of the sedimentation velocity of magnesium oxide and potassium dihydrogen phosphate depending their particle size, according to Stokes' law. The main particle sizes (measured by laser granulometry) are recalled for reference.*

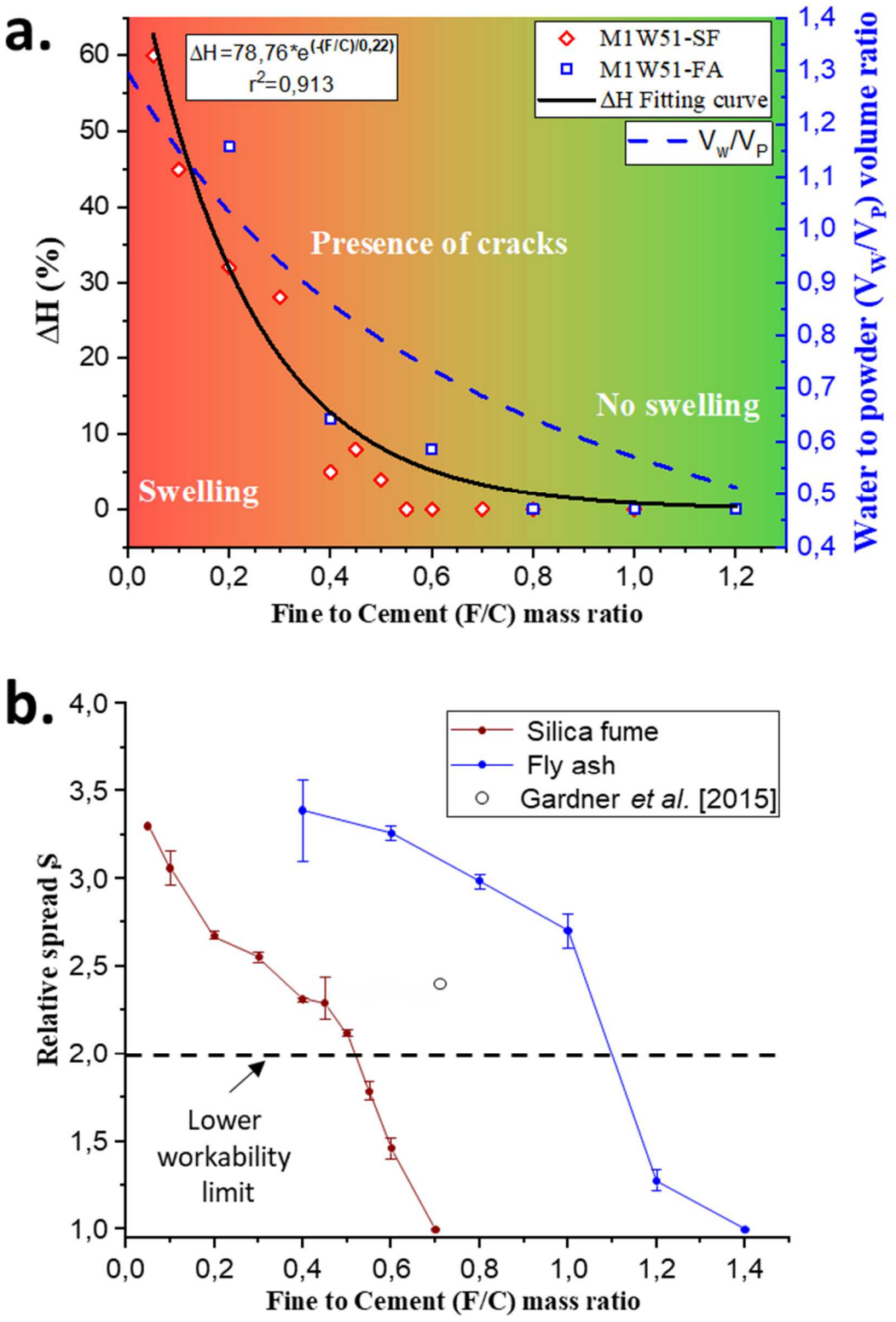

Figure 7: *(a.) Relative volume change ΔH and water to powder volume ratio (V_W/V_P) as a function of the fine-to-cement (F/C) mass ratio and (b.) Relative spread evolution of MKPC pastes added with FA or SF, depending on the fine-to-cement (F/C) mass ratio, compared with results from Garner et al.* [1] *(Mg/P=1.7, F/C=0.71, 3% of H_3BO_3 by weight of cement and W/C=0.41).*

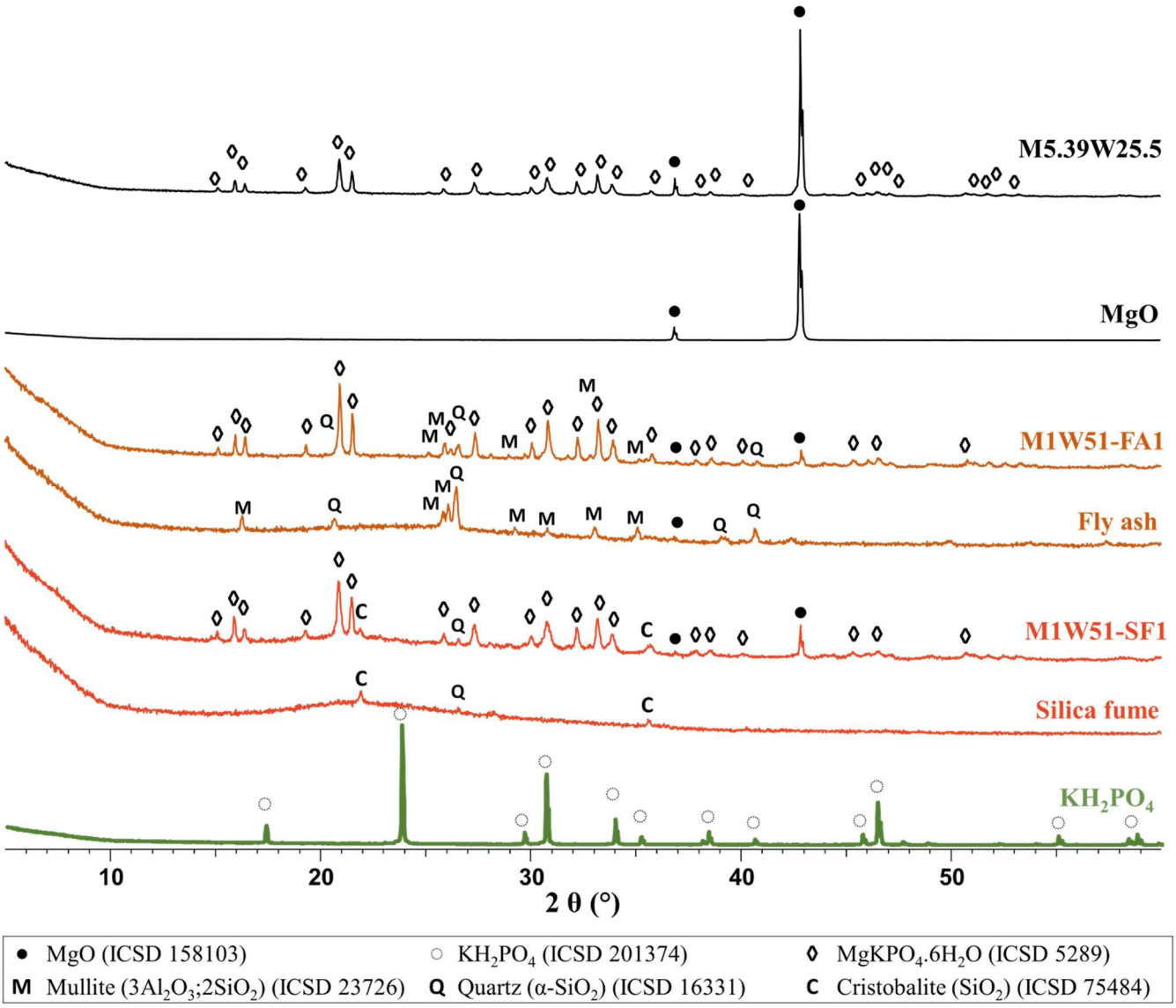

Figure 8: *XRD spectra after 28 days endogenous curing of the homogeneous* ***M5.39W25.5***, ***M1W51SF1*** *and* ***M1W5-FA1 MKPC*** *pastes.*

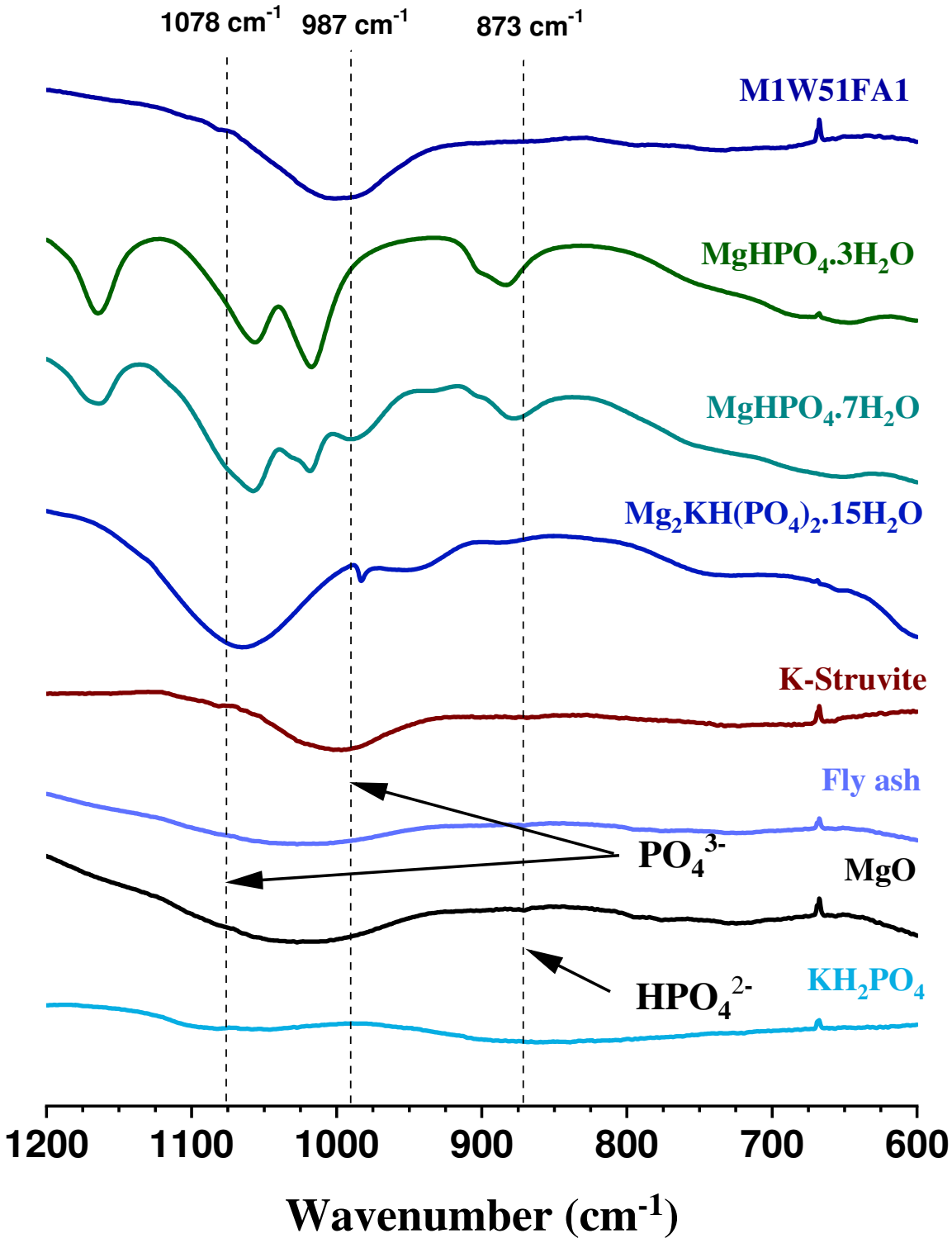

Figure 9: *FTIR spectra of the stoichiometric cement paste with fly ash (**M1W51FA1**) and of the different phases involved in Struvite-K formation, all tested after 28 days endogenous curing. Pure $MgHPO_4.3H_2O$, $MgHPO_4.7H_2O$, $Mg_2KH(PO_4)_2.15H_2O$ and struvite-K are synthetized independently and characterized by both XRD (to check for purity) and FTIR.*

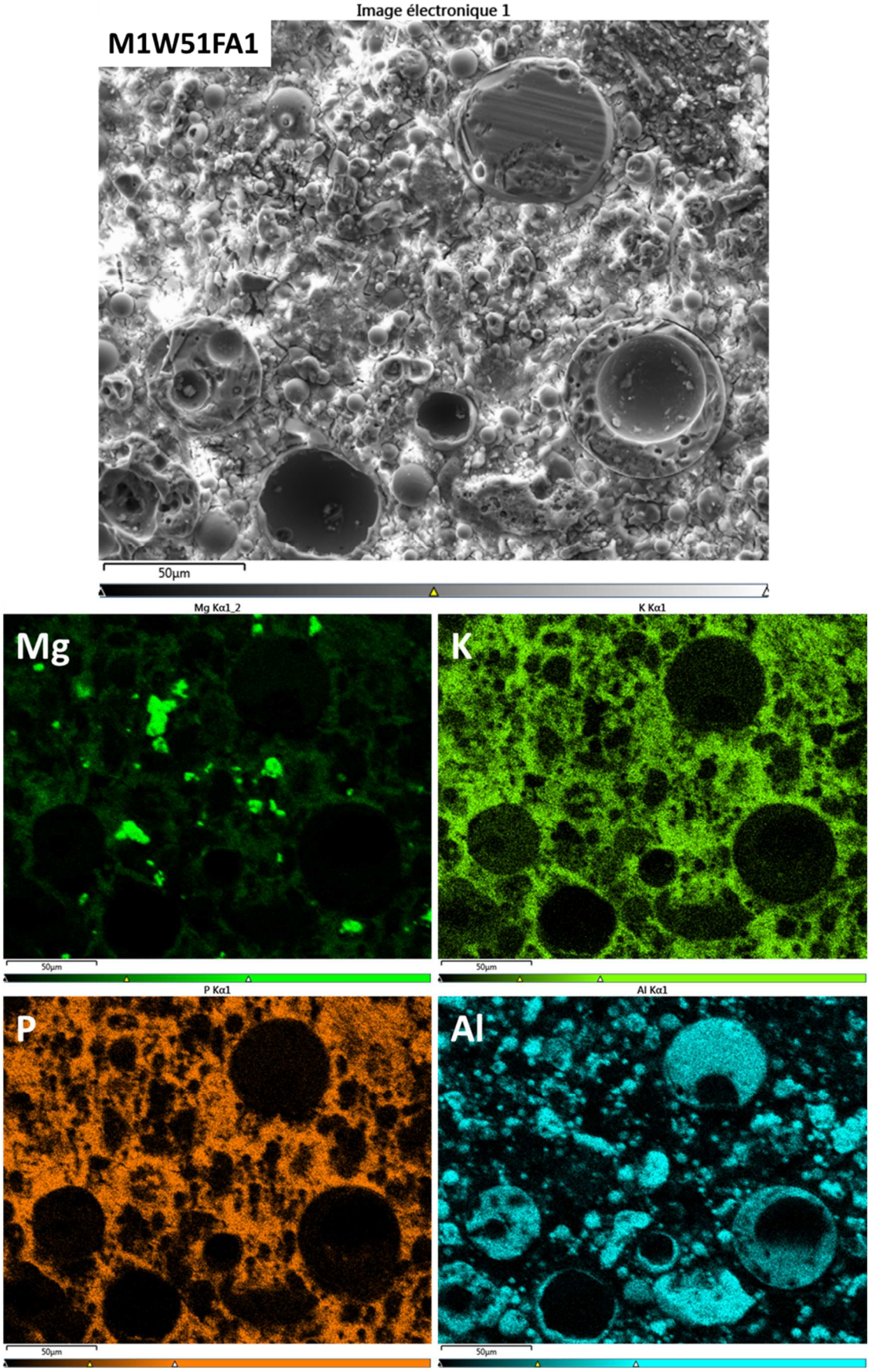

Figure 10: *Elemental cartography by EDX of the stoichiometric* ***M1W51FA1*** *paste with FA fine addition at 28 days endogenous curing, over an area of 250 µm x 200 µm*

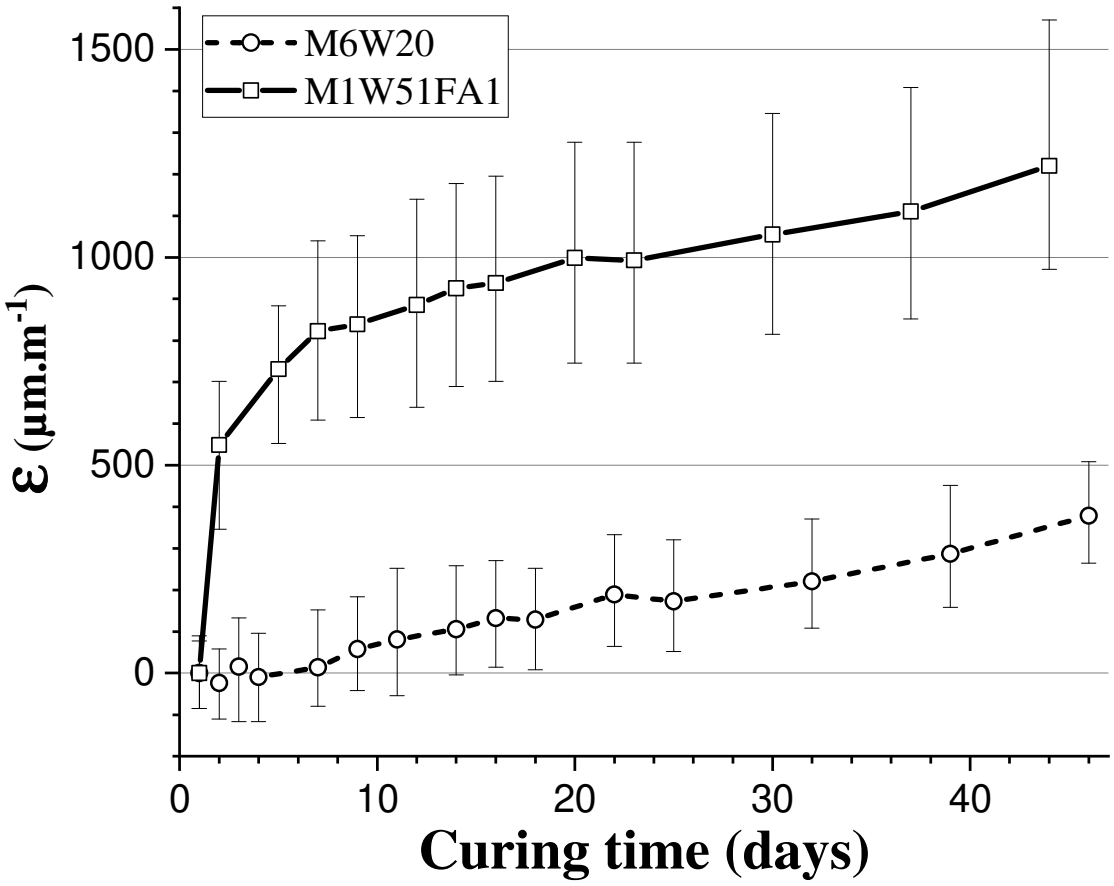

Figure 11: *Length change measurement (expansion) of* ***M6W20*** *stoichiometric* ***M1W51F1*** *cement pastes as a function of endogenous curing time.*

Supplementary materials

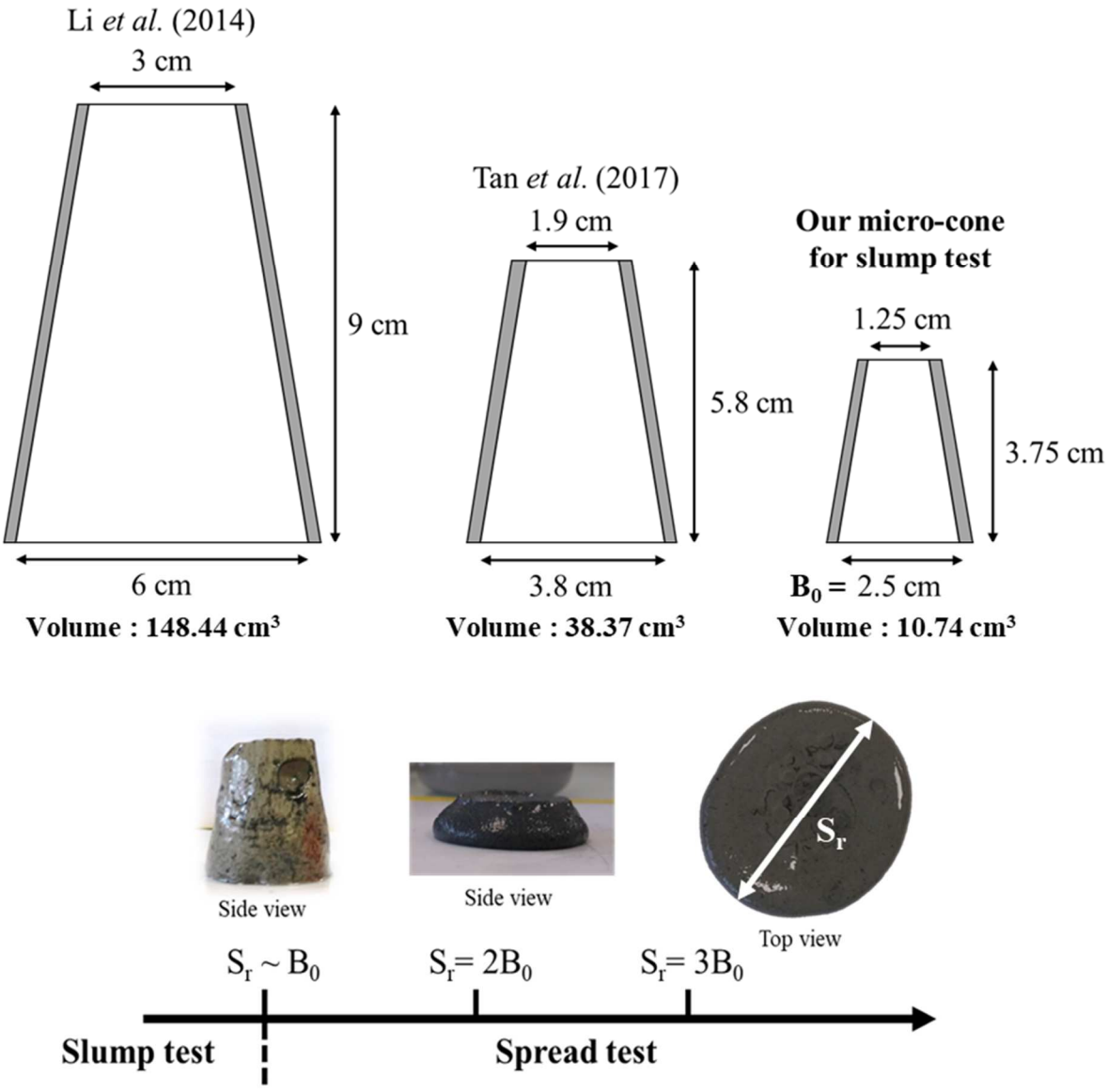

Figure S1: *(Top): Comparison between micro-slump test devices from the literature and the slump/spread micro-cone used in this research for rheological behaviour characterization; (Bottom): scale used for relative slump/spread measurements*

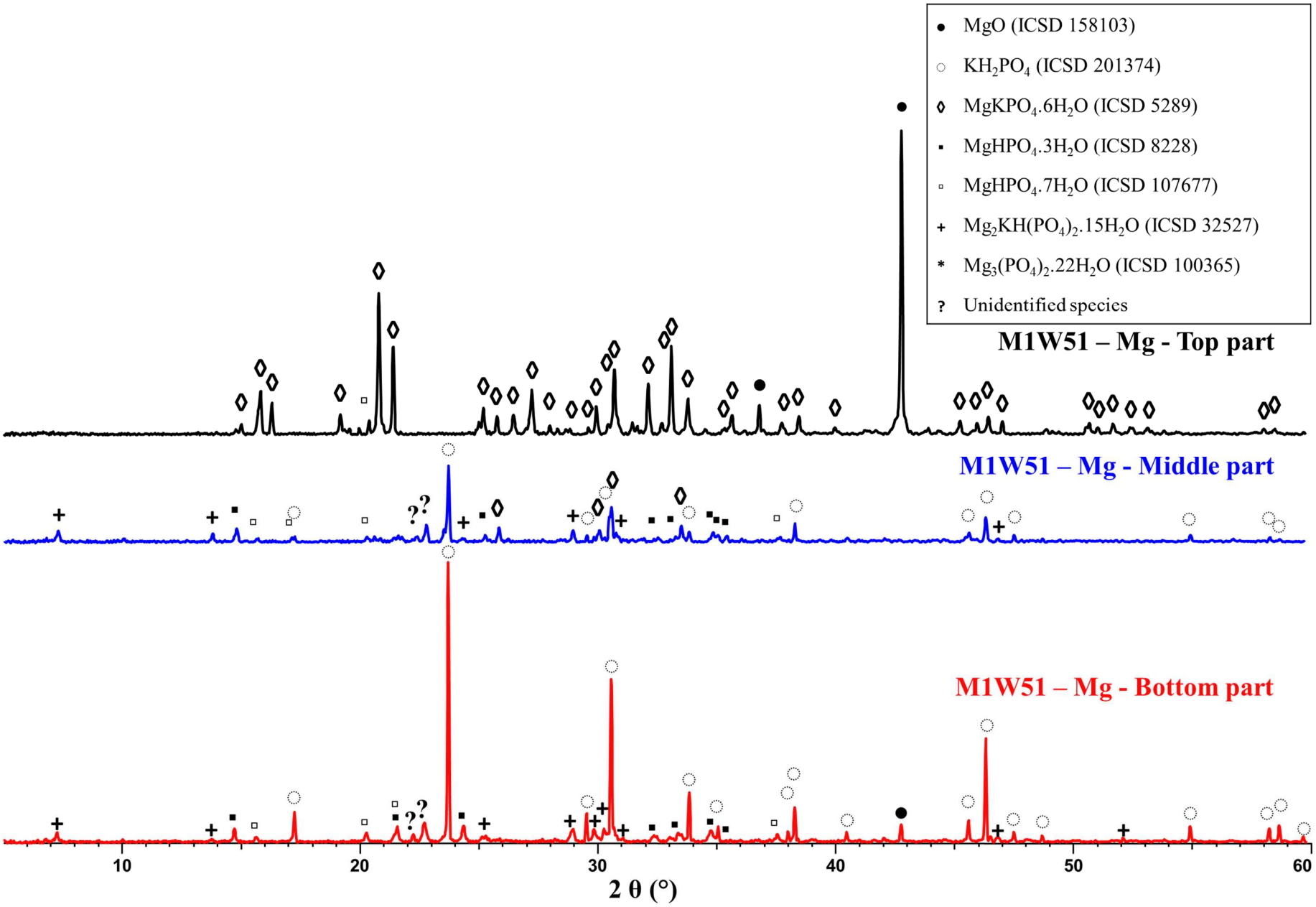

Figure S2: *XRD spectra after 7 days endogenous curing from the 3 parts of stoichiometric matrix* ***M1W51-Mg****.*

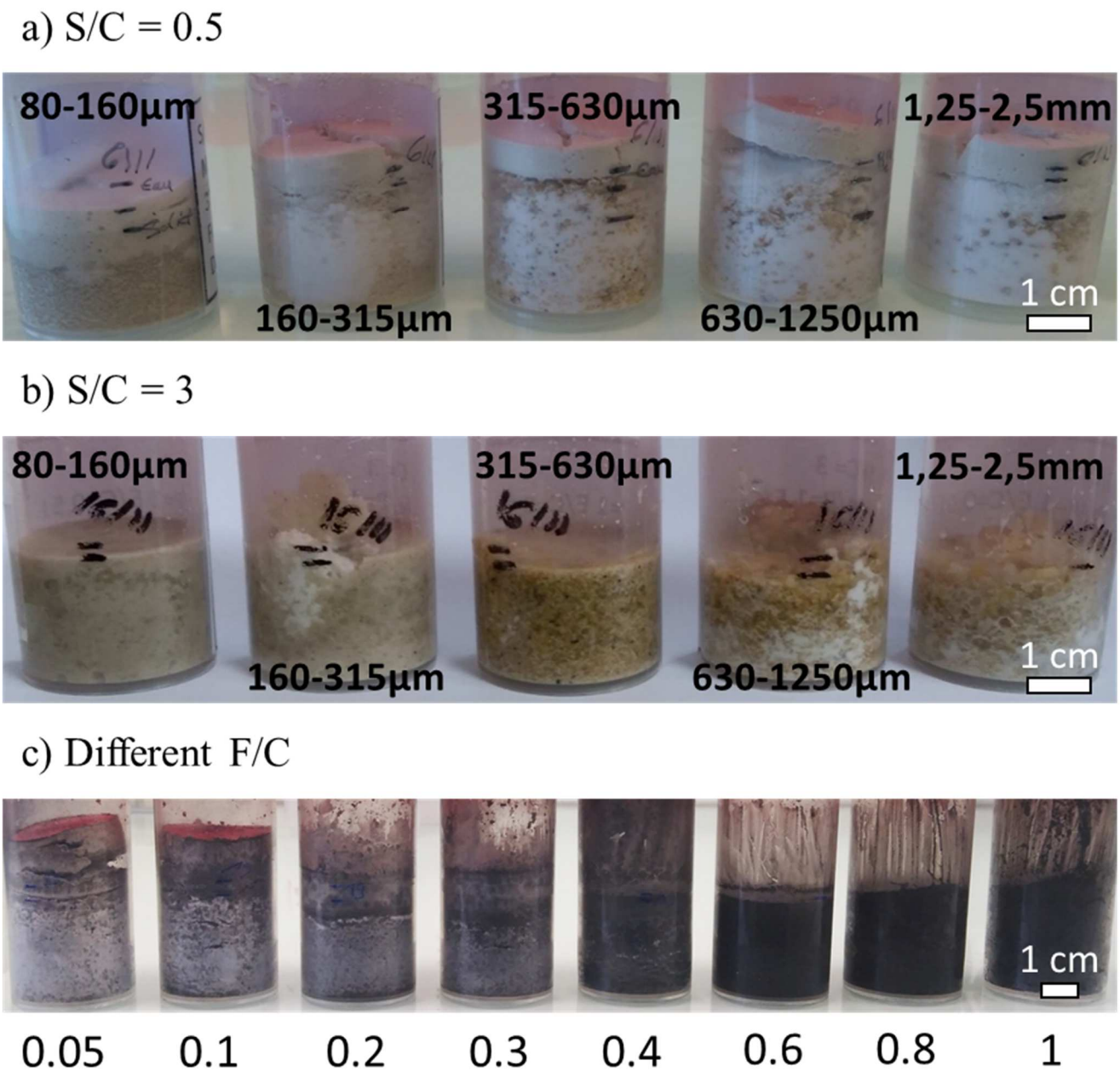

Figure S3*: Macro-photographs of different stoichiometric samples with (a and b) sand additions and two sand-to-cement S/C mass ratios of 0.5 (a) and 3 (b), and with (c) SF addition, for different fine-to-cement F/C mass ratios. Results for samples in a and b are detailed in Table 5, and for samples (c) in Figure 8b.*

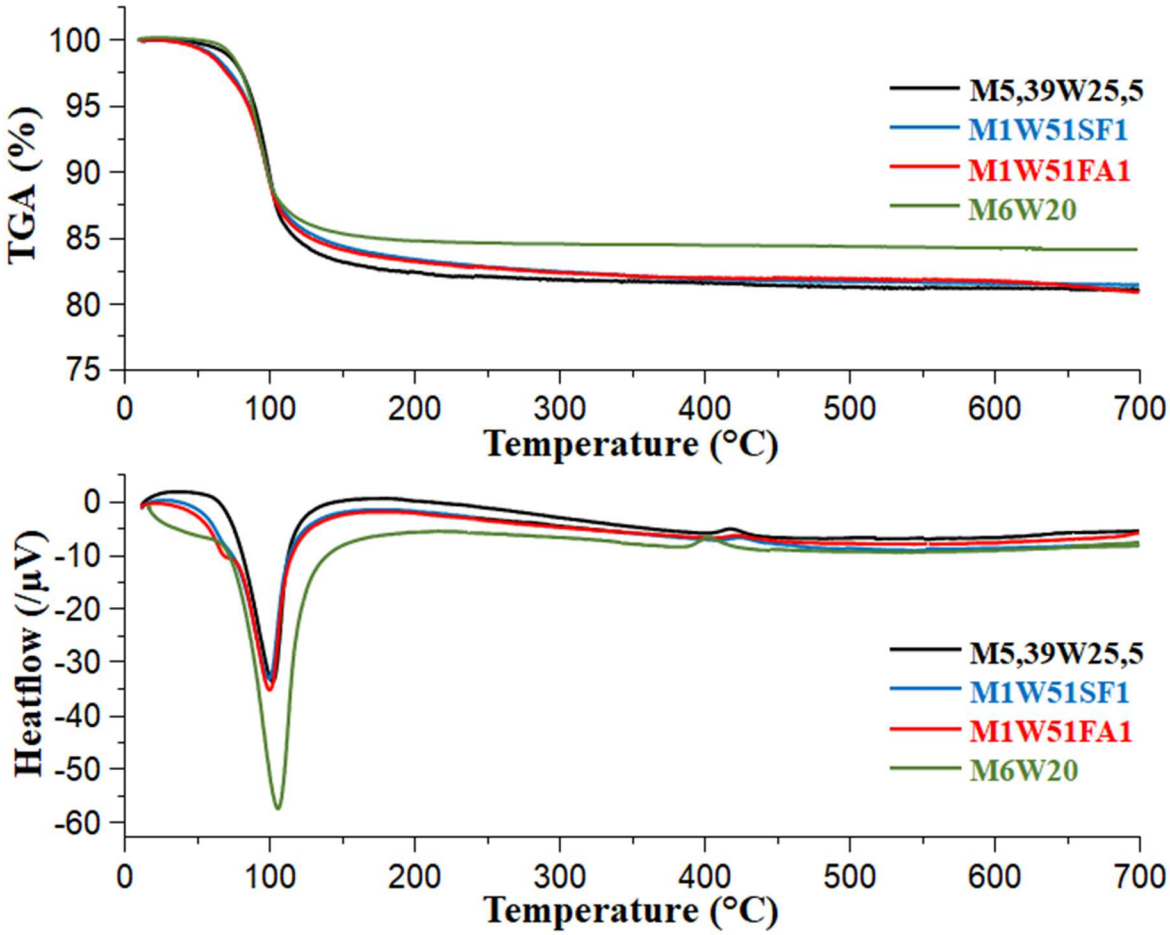

Figure S4: *TGA-DTA analysis for the homogeneous cement pastes* ***M5.39W25.5****,* ***M1W51SF1*** *and* ***M1W5FA1*** *after 7 days endogenous curing.*

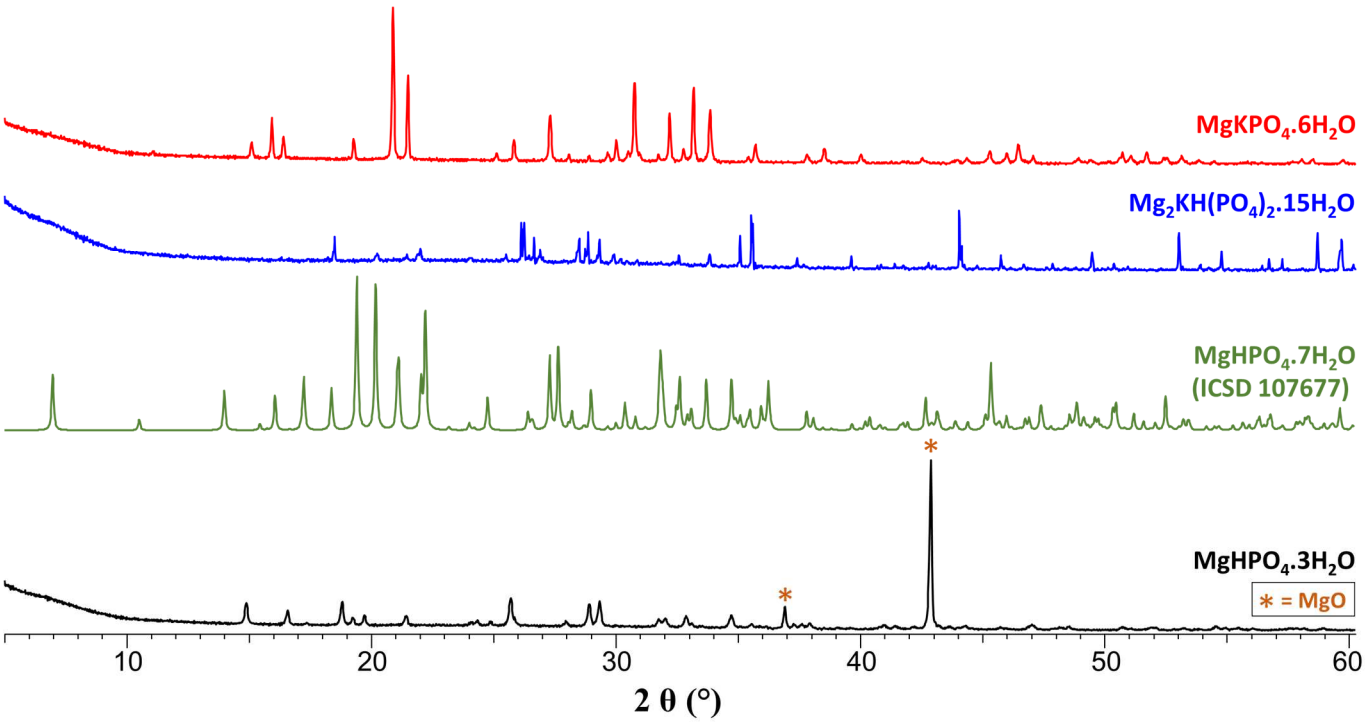

Figure S5: *XRD spectra of synthetized pure phases $MgHPO_4.3H_2O$, $Mg_2KH(PO_4)_2.15H_2O$ and struvite-K.*

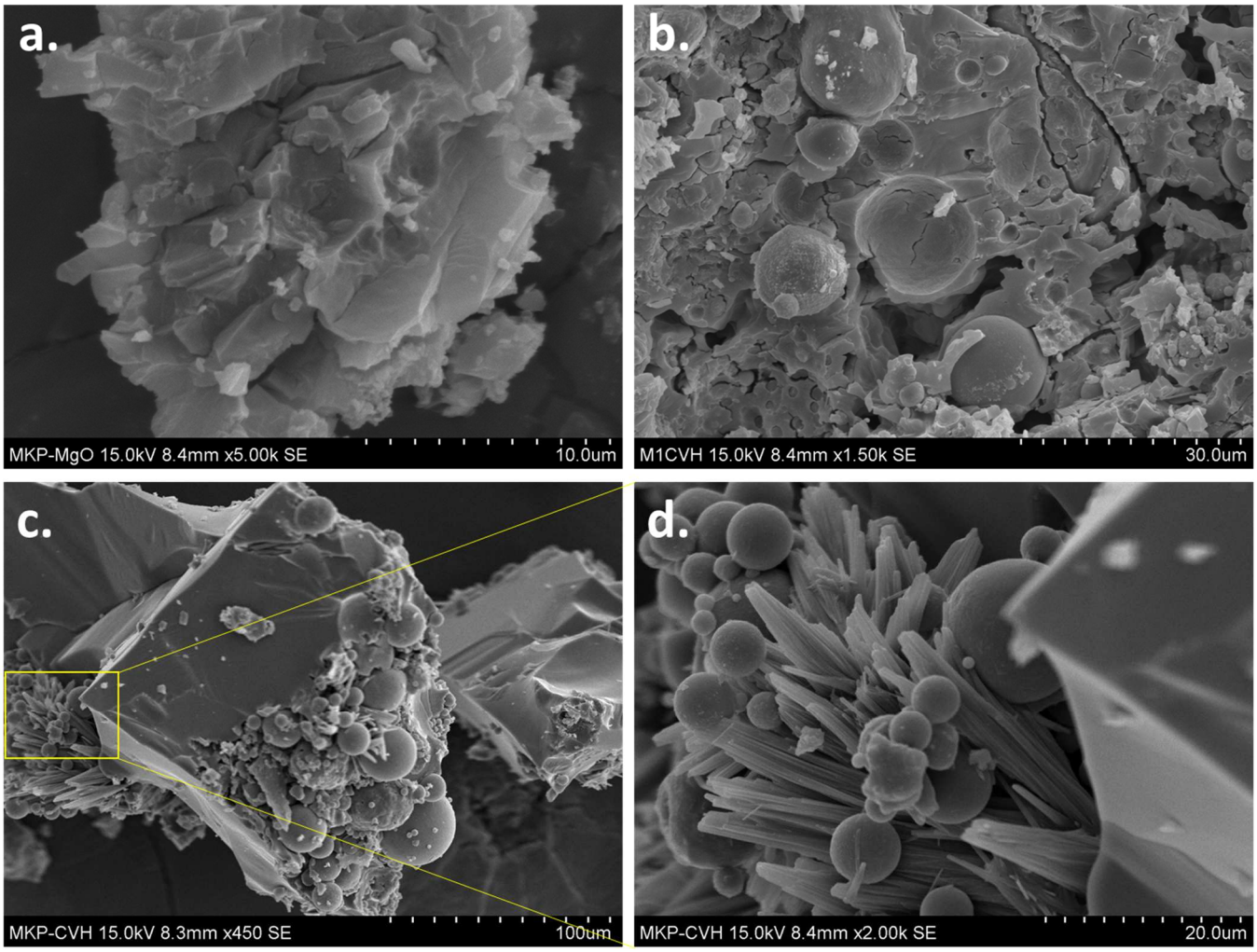

Figure S6: *Fracture surface observation by SEM of (a.)* ***M6W20*** *cement paste; (b.), (c.) and (d.)* ***M1W51FA1*** *cement paste. Both pastes are aged 28 days, and cured in endogenous conditions before failure in uniaxial compression.*